Forces in Mechanics 14 (2024) 100255

Contents lists available at ScienceDirect

Forces in Mechanics

journal homepage: www.sciencedirect.com/journal/forces-in-mechanics

A review of additive manufacturing capabilities for potential application in offshore renewable energy structures

Fraser O'Neill, Ali Mehmanparast *

Department of Naval Architecture, Ocean and Marine Engineering, University of Strathclyde, Glasgow G1 1XQ, Scotland, United Kingdom

ARTICLE INFO

Keywords:
Additive manufacturing
Offshore renewable energy
Fatigue, Corrosion
Erosion

ABSTRACT

Offshore renewable energy structures are subject to harsh environments with loading from wind, wave, and tides which introduce fatigue damage in corrosive and erosive environments. An effective approach that has been found to improve mechanical and fatigue resistance of engineering structures is employment of Additive Manufacturing (AM) technology. However, little research has been conducted for implementation of AM technology in offshore renewable energy structures. This study aims to collate and critically discuss the advantages that AM technology can offer to enhance the lifespan of offshore renewable energy structures. In addition to fatigue life improvement, the potential of AM technology to enhance corrosion and erosion resistance in offshore renewable energy structures has been explored. It has been found in this study that among the existing AM techniques, Wire Arc Additive Manufacturing (WAAM) offers promising potentials for life enhancement of offshore wind turbine and tidal turbine support structures. Early research into the potential of using WAAM to create corrosion resistance coatings and components highlights many benefits achieved from this new emerging manufacturing technology, but further research is required to justify the use of the processes for commercial applications. In terms of erosion and wear resistance even less research has been conducted but initial findings show that AM has the potential to add a great level of resistance compared to the wrought material. This study presents the key advantages that AM technology offers to enhance the design life and integrity of offshore renewable energy structures as a first step towards unlocking the great potentials of AM for consideration and implementation in the energy transition roadmap.

Introduction

With the need to move to a green energy system to meet the net zero targets, offshore renewable energy technologies are becoming of great interest. Scotland has ambitious Net Zero Targets to reduce emissions by 75 % by 2030 and complete Net Zero by 2045 [1]. To do this the Scottish Government is looking to create 11GW of offshore wind by 2030 [2] and have a pipeline of 27.6GW of offshore wind from their ScotWind leasing round [3]. The UK has a Net Zero target of 2050 and a target of 50GW of offshore wind by 2030, of which 5GW will be floating [4]. In offshore renewable energy sector, there are a variety of electricity generation methods from Offshore Wind Turbines (OWT), Wave Energy Converters (WEC) and Tidal Energy Converters (TEC). Each of these categories have both floating and fixed configurations. As of 2021 there was 34 GW of installed offshore wind globally, which is estimated to rise to 2002 GW by 2050. In ocean energy, there is 10.6 MW of tidal stream, and 2.31MW of wave; this is projected to rise to a combined 352GW globally by 2050 [5]. As these sectors grow it is important to understand their main degradation methods. For OWT, WEC, and TEC fatigue is a considerable issue along with extreme loads for wind and waves [6,7-9]. Corrosion is another major factor in the degradation of offshore structures and can seriously affect the life of the structures. Another degradation mechanism is erosion, but this is seen more in the blades of TEC and OWT. These structures have a typical life span of 20–30 years and therefore considering their degradation in the design phases is crucial [10,11]. For OWT life extension is becoming an area of interest with developers looking to increase the operational life of over one thousand turbines in the UK alone which will reach the end of their initial design life in the next decade.

The Levelised Cost of Energy (LCOE) is a common metric used in the renewable energy sector to evaluate the cost of energy of different technology types. Eq. (1) is used to calculate this where Capital Expenditure (Capex), Operational Expenditure (Opex) and Energy Generation (E_t) in a year (t) is used along with a discount rate (r) and

* Corresponding author.
E-mail address: ali.mehmanparast@strath.ac.uk (A. Mehmanparast).

https://doi.org/10.1016/j.finmec.2024.100255
Received 20 December 2023; Received in revised form 16 January 2024; Accepted 16 January 2024
Available online 17 January 2024

operational life (n) to calculate it. This in turn means that reducing either CAPEX or OPEX and/or extending the life cycle of offshore renewable energy assets reduces LCOE. Offshore wind has managed to do this in the last decade, as seen in Fig. 1 which details the LCOE within the offshore industry between 2010 and 2020, reducing from an average of $0.162/kWh in 2010 to $0.084/kWh in 2020.

$$LCOE = \frac{\sum_{t=0}^{n} \frac{I_t + M_t}{(1+r)^t}}{\sum_{t=0}^{n} \frac{E_t}{(1+r)^t}} \quad (1)$$

In 2019, the estimated foundation CAPEX for a 1GW farm using monopiles were ~£150 million and ~£310 million using jacket foundations. At the same time Operations and Maintenance (O&M) made up 28.3 % of the estimated LCOE [12]. Although these costs have reduced over time, they still have the potential for further improvement. However, the expertise in offshore wind gives hope to other renewable sources such as tidal and wave which need a reduction in LCOE to become more desirable investments. Fig. 2 highlights this by showing the current variation in LCOE for different offshore renewable energy sources.

Just like the renewable sector the additive manufacturing (AM) sector has seen a surge in interest in the last few decades and exponential growth since the early 2010's, Fig. 3 highlights this by showing the revenue from both products sold and services provided between 1992 and 2022. This is due to the advances in the technology and the advantages it brings such as being able to create complex geometries easily in much shorter timescales compared to the traditional manufacturing methods, Near Net Shape, reduction on material wastage, reduction in part count for assemblies, reduction in energy and reduction on lead times.

This growth of AM technology has no sign of slowing with the global revenue forecast to be ~$102.7 Billion by 2032, as shown in Fig. 4 which shows global revenue from 2016 and forecasted global revenue to 2032. The AM technology has been of particular interest to the automotive and aerospace industries as parts with complex geometry are easily achieved in quick lead times. This can be seen from the revenue stream break down for different industries suppliers have served illustrated in Fig. 5. An excellent example of AM being utilised in aerospace is the Relativity Space Terran 1 rocket where 85 % of the mass was made from AM. The main body is produced via Wire Arc Additive Manufacturing (WAAM) making it the largest AM structure as of 2022 with a diameter of 2.28 m and height of 33.5 m [14]. With the energy sector there has been a slower uptake and is more commonly utilised within the nuclear industry. This is due to confidence in the technology being achieved after Siemens used AM to create an impeller for a fire protection pump at their Krško nuclear plant in Slovenia. Now AM has an addressable market of $40 billion in the nuclear industry as of 2020. The wind industry is also starting to look at AM for creation of large-scale moulds for blades, concrete foundations and retro design of discontinued parts. It is estimated that by 2030 the addressable market of AM for wind will be $44 billion [15].

AM has the potential to play a role within the structural elements of wind turbines for both repair and manufacture. Oak Ridge National Laboratory (ORNL) has carried out an investigation into structural nodes for the Vesta wind turbines. In this investigation both composite and WAAM techniques were used to evaluate their potential to meet the system requirements. From this WAAM was shown to be the best method, outperforming the structural requirements of the part. The study also found that the WAAM process reduced lead time by 95 % but the cost was 14 times higher than that of steel welded parts [16]. WAAM is one of the most promising technologies in AM for offshore renewable structures due to its ability to create large, complex parts in short lead times. As such DNV have created standard DNV-ST-B203 which is a qualification standard for AM for the oil and gas and related industries which focuses on WAAM and Laser Based Powder Bed Fusion (L-PBF) processes. Ole-Bjørn et al. [17] carried out a case study for the standard looking at a circulating head built from WAAM. The standard states that a sacrificial component should be produced for testing along with the production component. The production part itself should also have a prolongation that can be utilised for testing. In this study these where both produced and tested as shown in Fig. 6 where the mechanical requirements for the part have been exceeded. The study concluded that both WAAM and the standard are fit for purpose within the offshore industries.

Among a wide range of existing AM methods, this study aims to focus on the potential of the WAAM technology due its capability for production of large-scale structures, in offshore renewable energy components and structures; detailing how through the WAAM process, materials can be combined to combat against environmental and operational conditions. A lack of knowledge in the degradation of WAAM materials in terms of fatigue, corrosion and erosion is also discussed detailing how improvements in these areas can help in longer design life and the life extension of the future and current offshore renewable

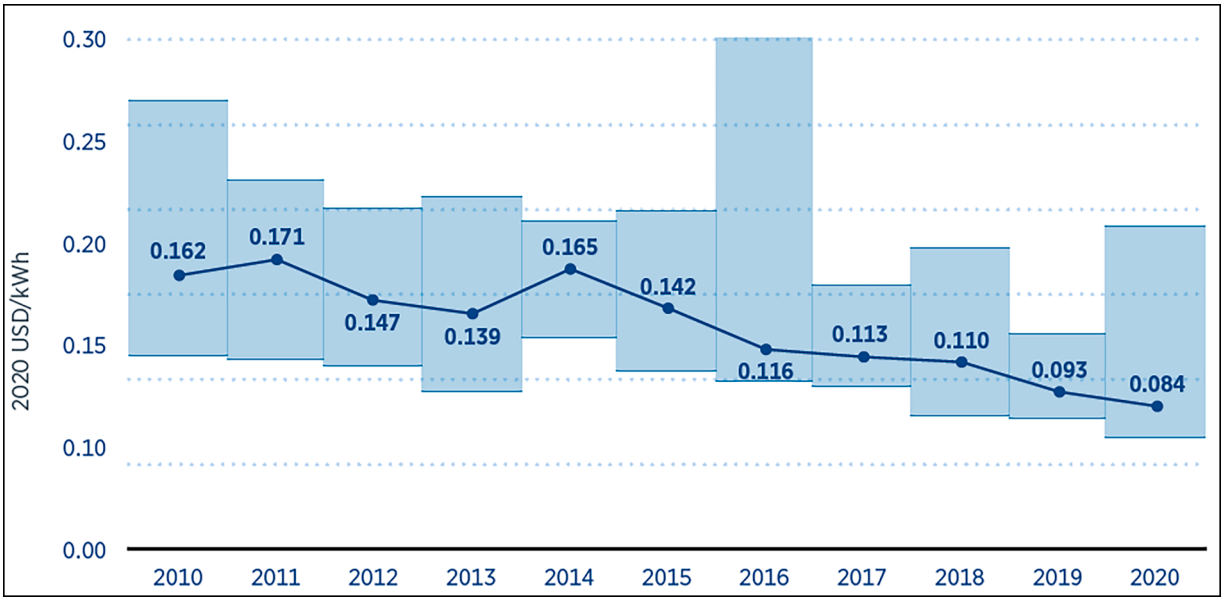

Fig. 1. LCOE of Offshore Wind, 2010–2020 [5].

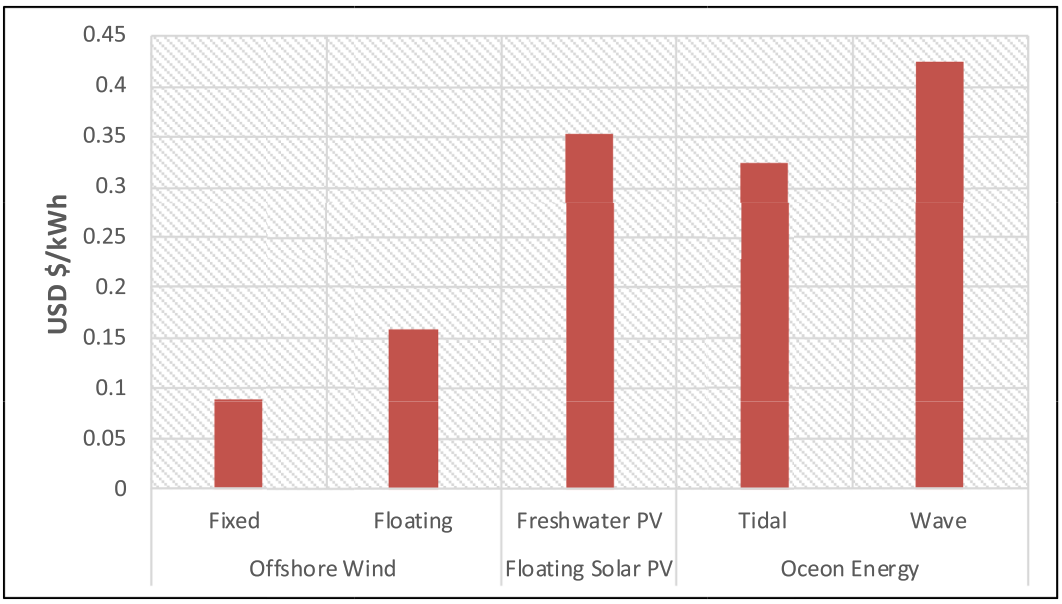

Fig. 2. LCOE Comparison of Offshore Renewables (2019–2020) [5].

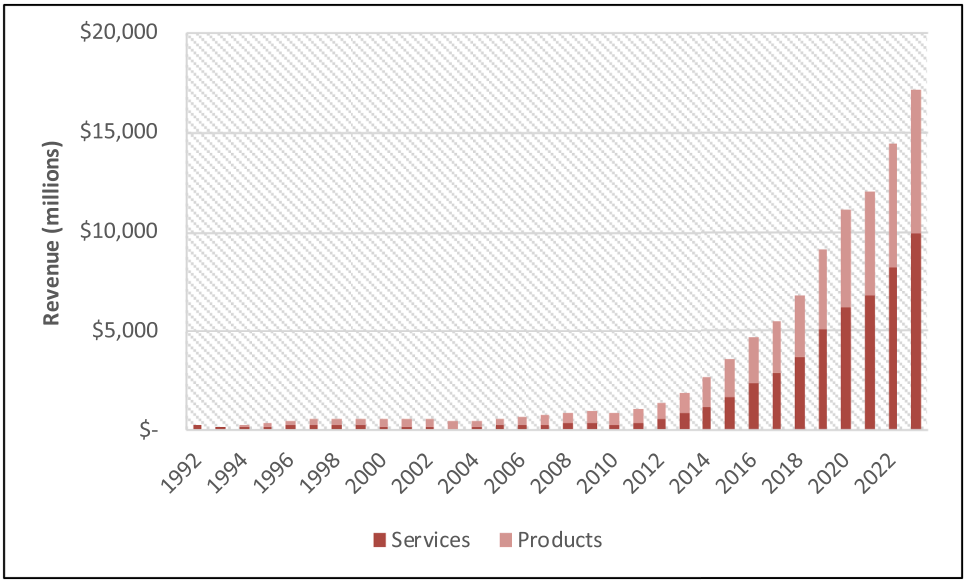

Fig. 3. Overall AM Industry Revenues 1992–2022 [13].

energy structures' life cycle.

Range of AM technologies for marine applications

Although many associate AM with the age of computers, the first AM technique was patented in 1920 with the WAAM process designed for creating artistic pieces [18]. The first commercial printers emerged in 1987 from 3D Systems that used stereolithography (SL), a process that uses lasers to cure liquid polymer material [19]. Today AM has come a long way with a wide range of methods that can be utilised. These are often classed into seven categories which within each are several other processes, as demonstrated in Fig. 7.

When looking at offshore applications metal processes will likely be the focal point in terms of AM. ASTM 52900 details the metallic processes available to date, Fig. 8 breaks these down via different stages of the manufacturing process. Sheet Laminate, also called, Laminated Object Manufacturing (LOM), is a process in which sheet material is cut and layered with either rolling, ultrasound or bonding applied to each layer. Sheet Laminate is unlikely to be commonplace in the offshore environment due to issues with time consuming post processing, limited material options and bad dimensional accuracy. However, it can be useful for the prototyping of concepts [13,20]. The two processes which are most likely to be used in the production of parts for the offshore environment are Powder Bed Fusion (PBF) and Directed Energy Deposition (DED). PBF only uses a powder material whereas DED can use both powder and wire feedstocks.

PBF is a method in which a power source, either laser, thermal or electron beam, is used to fuse together material power to create a layer. These processes include Selective Laser Sintering (SLS), Selective Laser Metling (SLM) and Electron Beam Melting (EBM). The processes yield excellent Near Net Shape and complex geometry and a wide range of material options. However, due to the nature of the process high porosity, thermal stresses, poor density and limited build size leave these processes at a disadvantage [22]. This process has seen a lot of interest in

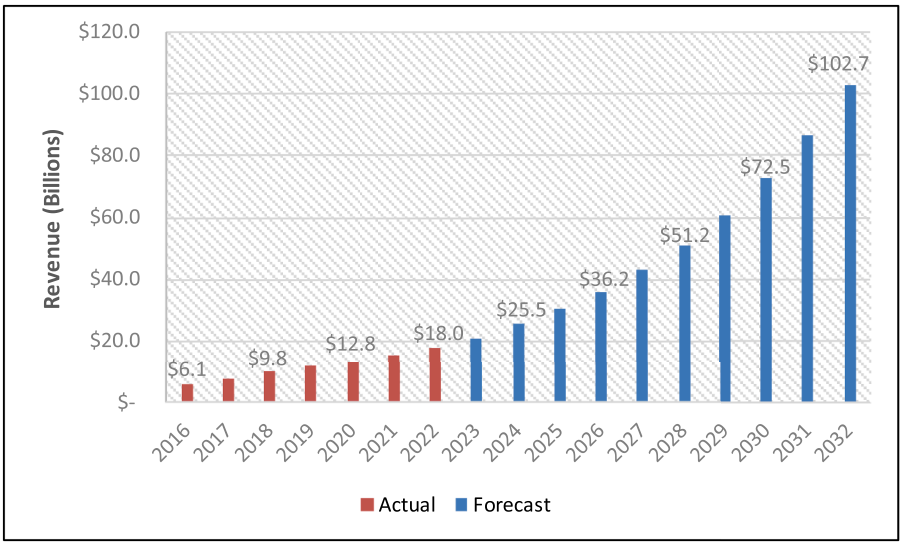

Fig. 4. Global AM Market Forecast as of 2022 [13].

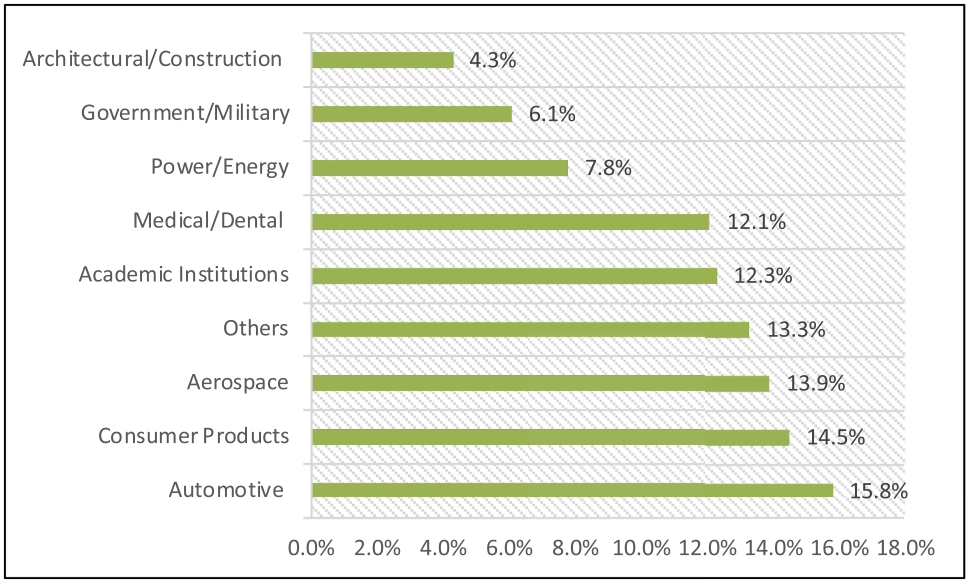

Fig. 5. AM Suppliers Revenue Percentage by Industry [13].

the energy sector with Siemens winning an Emerging Technology award from American Society of Mechanical Engineers (ASME) for their work on creating gas turbine blades from AM, these can be seen in Fig. 9 [23]. The creation of the DNVGL-ST-B203 which looks at both PBD and DED processes showcases the potential and intertest for the technology in the offshore environment.

DED is the process of using an energy source to melt material at the energy source, either, electric arc, electron or laser, allowing the melted material to be deposited onto the build surface. This is usually carried out using a robotic arm, with some variants having a moveable build plate to increase degrees of freedom and enables the creation of large parts. This is one of the main advantages of the process, as size constraints are minimised due to the flexibility of the robotic arm. DED can be further categorised by either powder or wire feedstock. Powder DED can lead to similar issues in terms of porosity as PBF, whereas wire feedstock has lower porosity issues. WAAM can deliver some of the highest deposition rates at minimal energy compared with PBF processes. An example of this being used within the maritime industry is the manufacture of large, high-quality propellers for the ship building industry. The French Navel group investigated the possibility of using this for their mine sweeper class and found WAAM built propellers, an example of which is demonstrated in Fig. 10, allowed for a much higher quality, higher strength at minimal waste compared to the traditional cast options [24]

Within the literature there is currently no examples of WAAM parts being used in ORE industry. This could be down to the maturity of the process and the need for further testing on the process to validate it is fit of purpose. In academia studies have been conducted looking at the properties of a range of materials in terms of fatigue and mechanical properties. However, in general ER70S-6 and ER100S-1 are commonly analysed due to them being similar composition to S355 which is commonly used for offshore structures. There has been limited research regarding the corrosion resistance of WAAM material. However, preliminary studies have been conducted looking at the potential application of WAAM for ORE structures. One such study by Mehmanparast et al. compared ER70S-6 and a hybrid of ER70S-6 and ER90S-B3 in terms of fatigue performance after exposure to a corrosive environment. From this they have shown that corrosion dramatically reduces fatigue life but

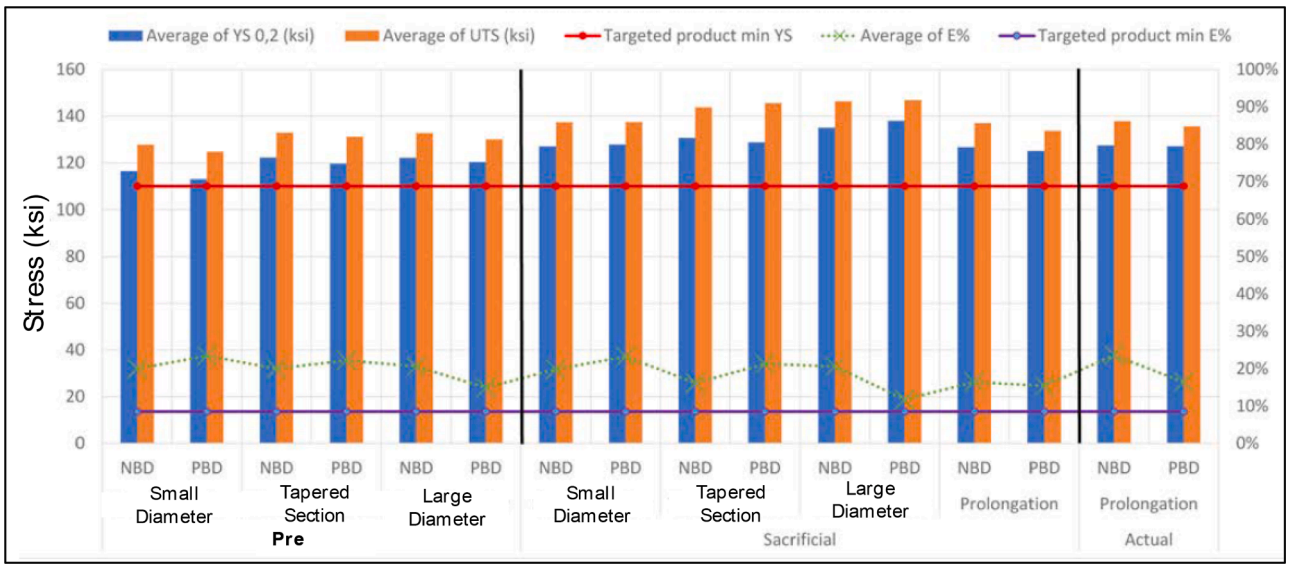

Fig. 6. Mechanical Properties of Circulating Head Built by WAAM [17].

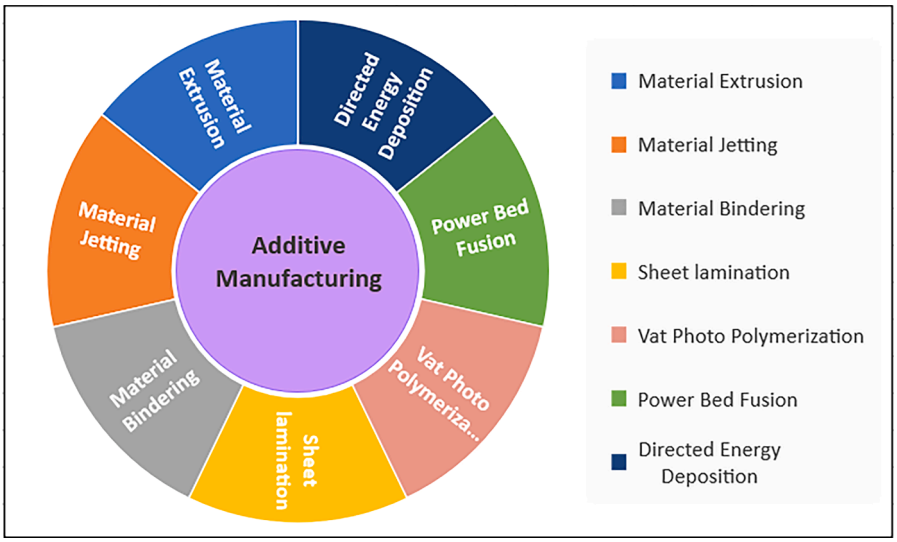

Fig. 7. Additive Manufacturing Classifications.

by combining the two materials to make a hybrid can enhance the fatigue life of material in both air and after corrosion when compared to the ER70S-6 [25]. No studies could be found that evaluate the impact of erosion on WAAM materials for ORE structures. Future work with industry is required to identify possible components that would be suitable, and benefit being partially or entirely manufactured from WAAM.

Enhancement of life limiting factors in offshore renewable energy structures using AM technology

Fatigue is described as a failure mechanism which occurs after a material experience's repeated cyclic loading. During these cycles microcracking occurs when the loading is greater than the fatigue limit of the material. Fig. 11 shows the step-by-step process of fatigue failure. From this it can be seen that the initiation period, during which the microcracking occurs, is the largest portion of the failure process, with the cracks being near impossible to detect. Once the crack is visible this is called the crack growth period and continues until failure.

Surface condition of a material severely affects the fatigue life of a metallic structure. Erosion is the term given to a range of surface damage mechanisms that occur when a surface is impacted by solid or liquid particles. These impacts can lead to the removal of material flakes, plastic deformation, fatigue cracking, melting around the impact site and degradation of the lattice structure of the material depending on a wide range of parameters. These include particle material, velocity, impingement angle and size. All these parameters influence the severity of damage arising from erosion. Fig. 12 showcases the damage mechanisms possible from erosion scenarios considering impingement angle, size and speed.

Corrosion is an electrochemical process in which electrons flows from the anode to the cathode via an electrolyte, Fig. 13 provides a diagram of this reaction, and in the case of offshore structures this is the aqueous environment. This results in the removal of electrons and in turn material loss. This occurs at the surface of the material and similar to erosion causes surface damage. Both erosion and corrosion can influence the fatigue life of a material as a result of the surface damage caused by the processes.

In terms of the structural integrity of OWTs, Floating Offshore Wind Turbines (FOWTs), TECs and WECs they all will experience cyclic loads coming from wind, wave and tides during their operational lifespans,

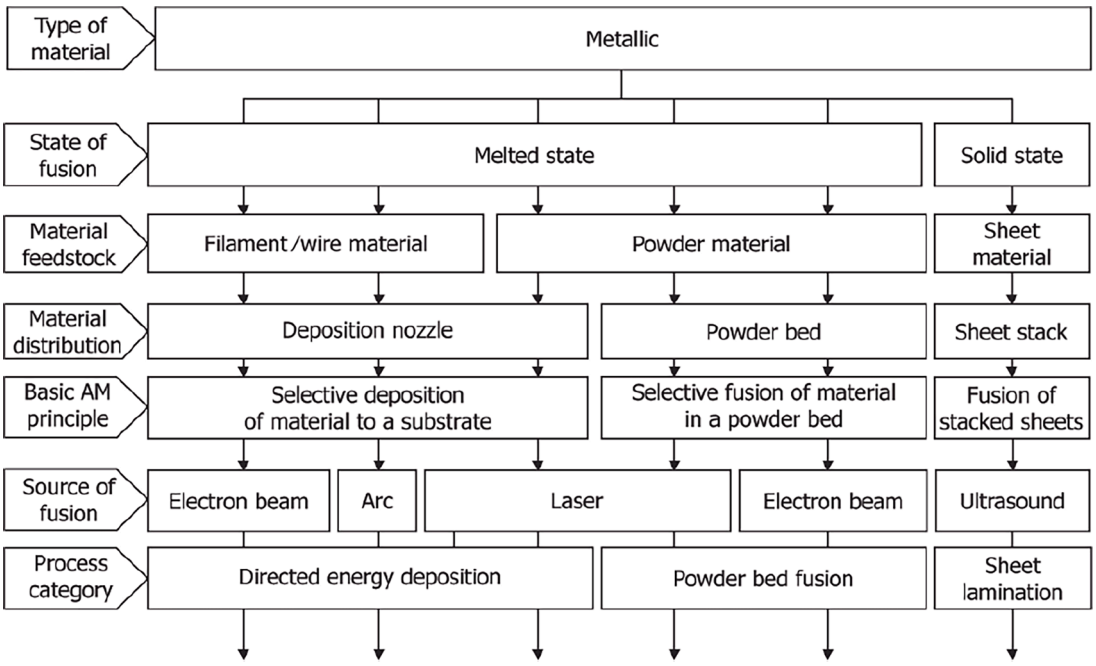

Fig. 8. Overview of Single-Step AM Processing Principles for Metallic Materials [21].

Fig. 9. Gas Turbine Blades made for Siemens by Material Soultions [23].

Fig. 10. Propeller Created via WAAM Manufactured by French Navel Group [24].

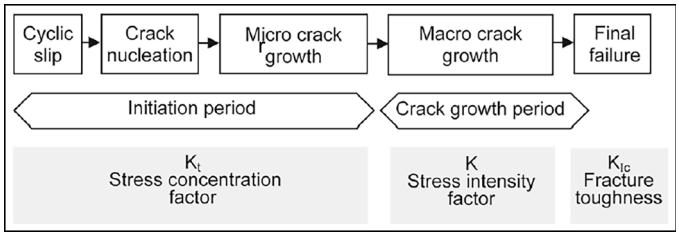

Fig. 11. Different Phases of the Fatigue Life and Relevant Factors [26].

hence fatigue damage due to the nature of the marine environment. However, fatigue damage is not the only degradation mechanism in offshore renewable energy structures as it can interact with other environmental damage mechanisms such as corrosion and erosion, which results in reduced fatigue lives and accelerated crack growth rates. The same can be said for corrosion and erosion as they can also interact with other material degradation and damage mechanisms. For example, TECs experience erosion more than other renewable sources due to operating near the seabed in fast flow speeds with sand particles in the flow. This erosion can interact with corrosion and fatigue damage mechanism to decrease the structures life. Therefore, to enhance the structural design and life expectancy of offshore renewable energy structures, the level of damage occurring from each of these potential mechanisms must be reduced both in isolation and combination. These life improvements can be hypothetically achieved by employing AM technology in offshore renewable energy structures, a great potential of which is comprehensively explored next.

AM potentials for corrosion resistance

Grasu et al. carried out a complete risk assessment of FOWT structures using case studies, data and industry expertise input. The assessment has shown that corrosion is the biggest failure mechanism risk [29]. Corrosion causes surface degradation and eventually leads to either stress corrosion cracking or corrosion fatigue cracking. Orlikowski et al. investigated the effect of corrosion on carbon steel S235JR in the Baltic Sea from sea level down to the seabed at 75 m depth [30].

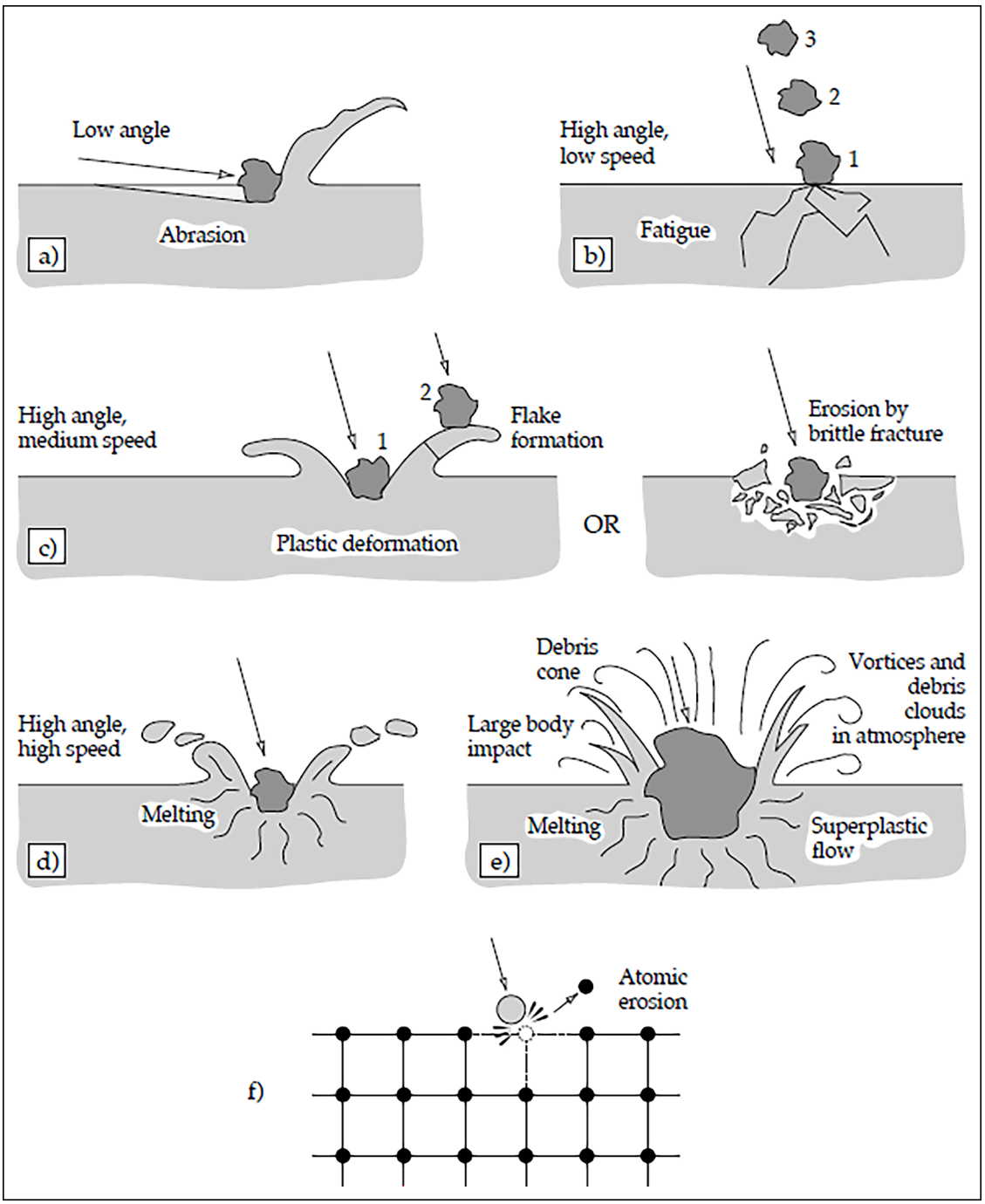

Fig. 12. Possible mechanisms of erosion; a) abrasion at low impact angles, b) surface fatigue during low speed, high impingement angle impact, c) brittle fracture or multiple plastic deformation during medium speed, large impingement angle impact, d) surface melting at high impact speeds, e) macroscopic erosion with secondary effects, f) crystal lattice degradation from impact by atoms. [27].

From this investigation it was found that seasonality has an influence on the corrosion rate along the water column. It was noted from Linear Polarization Resistance (LPR) analysis that the corrosion could be above 0.8 mm/year at the sea surface and 0.4 mm/year at the seabed. Samples were placed on an offshore production rig for 6 months in the immersion zone whereafter they were cleaned of organic material and the mass loss was recorded. From this the average corrosion rate was 0.355 mm/year was found which is lower than LPR analysis due to the organic and corrosion material slowing the corrosive wear. Another study on corrosive behaviour was carried out by Khodabux et al. but this time on samples in the North Sea looking at the varying depth with samples left in the sea for 111 days. Corrosion rates varied from 0.56 to 0.83 mm/year depending on the water depth. The highest corrosion rates were noted at the sea surface and seabed. A comparison of corrosion rates to the DNV J101 standard and field experiments at 43 locations worldwide was conducted in another independent research [31]. This showed that the highest corrosion rate from this was four times that of the J101 standard. The corrosion rates from the 43 sites were also considerably lower than measured values. However, no information on the type of experiments, materials, coating or depths were given for these results [31]. The results from these studies show the extend of uniform corrosion rates of uncoated metal coupons exposed to the marine environment and highlight the impact to the structural integrity of parts made of steel. The high risk nature of corrosion as a failure

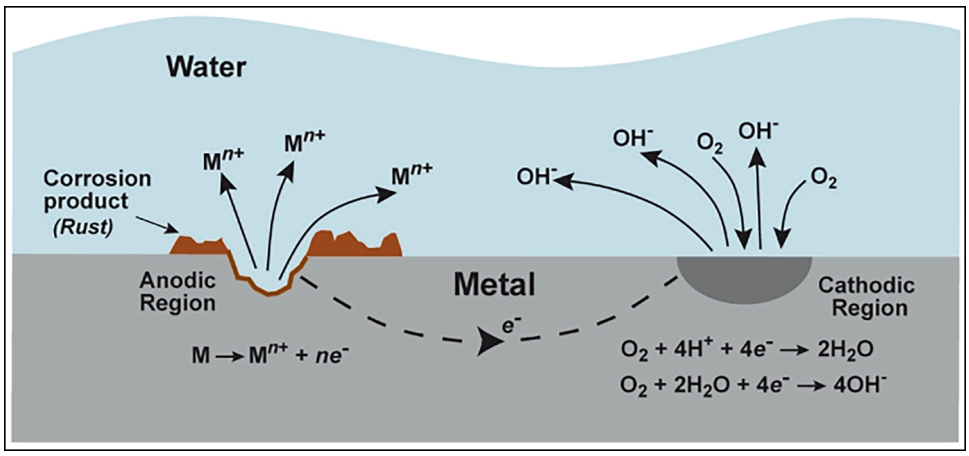

Fig. 13. A schematic diagram of a typical electrochemical cell formed during the corrosion of a metal M immersed in water [28].

mechanism showcases how creating structures with a long-life cycle or extension can only be achieved if the resistance to the corrosive environment is considered at the design and maintenance phases.

There are some studies which have been conducted into the corrosion effects of materials made from AM processes. Tian et al. looked at the microstructure and properties of Inconel 625 made via laser cladding against different composition and wrought material. This showed that through laser cladding, also called Laser Directed Energy Deposition (L-DED), the material showcased better corrosion properties to that of the wrought material and with the use of composition changes the material can be tailored for its application [32]. L-DED uses powder feedstock and requires high energy. This led to expensive manufacturing and issues with porosity. Rajkumar et al. studied Incoloy 825 via WAAM and found that the corrosion resistance of the material in 3.5 % NaCl solution was superior to that of the wrought material. They also highlighted that potentiodynamic polarization curves for material taken from different area of the WAAM built wall showed different corrosion resistance values [33]. Vishnukumar et al. investigated WAAM for aluminium repairs in marine environments. Results showcased similar corrosion rate to that of wrought material with excellent passivation leading to high corrosion resistance [34]. Rajesh Kannan et al. researched microstructure and corrosion resistance of Monel FM60 alloy via WAAM. They found that the corrosive resistance was better than that of wrought Monel 400 and that the pitting resistance was deemed outstanding. This was believed to be due to the Ni matrix remaining in the material enhancing corrosion resistance [35]. The team also conducted corrosion analysis on Super Duplex Stainless Steel (SDSS) manufactured via WAAM. Fig. 14 shows the pitting that occurred during testing at the bottom, middle and top of the wall. Their results found that the Pitting Resistance Equivalent Number (PREN) was great enough to meet oil and gas requirements and that the corrosion performance was greater than that of wrought [36]. In both investigations the corrosion rate of the bottom of the wall was superior to the top. Queguineur et al. created WAAM built Aluminium-Copper walls and compared them to wrought AISI 316 L. They found that the WAAM material had corrosion rates similar to cast and forged material with build times similar to traditional methods [37].

All these studies for WAAM in the marine environment have focused on highly corrosion resistance materials but they also incur a high cost. Most offshore renewable energy structures are made of structural steel with corrosion protection systems which fail periodically and need to be replated during which the corrosion damage will be induced into the material. Little studies have been done of structural steel via WAAM and the effects of corrosion on them. A. Ermakova carried out a study on ER70S-1 steel via WAAM looking at how corrosion effects the fracture mechanics of the material and it was discovered that the crack tip of the material was blunted by corrosion leading to corrosion improving the fracture toughness of the material [38]. From literature is it clear that due to the nature of WAAM the flexibility of control over composition and manufacturing process enables the tailoring of materials/components for different applications and has potential in the marine environment in terms of corrosion resistance.

AM potentials for erosion resistance

Erosion in offshore structures has not been heavily researched due to corrosion being seen at the main damage mechanism. However, in tidal stream energy erosion is seen as an issue due to their location near the seabed, high flow velocities and sand particles in the flow. Within the tidal energy industry research on erosion is mainly focused on the composite blades [39]. Even though erosion has been studied for tidal energy it is few and far between leaving a gap in the knowledge for

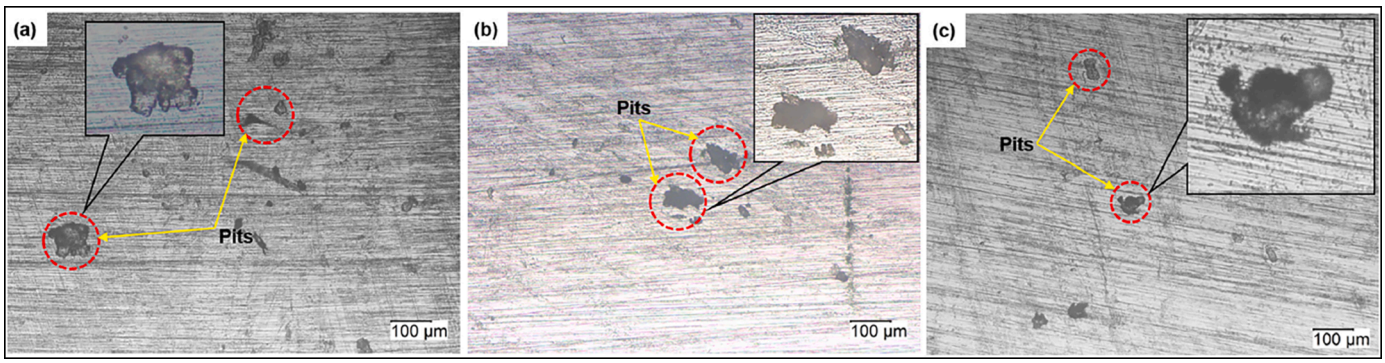

Fig. 14. Optical micrographs showing pits from samples at wall location: (a) Bottom, (b) Middle and (c) Top [36].

academia and industry. Effects of erosion has also been studied for ship building steel with Xu et al. investigating EH 32 carbon steel under erosion in natural seawater. Pure Erosion tests use cathodic protection to stop the influence of corrosion occurring and therefore only allow for erosion as a damage mechanism to the surface. Erosion tests were conducted and showed that at velocities lower than 5 m/s the mass loss is minimal. At 5 m/s a mass loss of only 0.60 mm/yr was recorded. This dramatically increases as flow increases to 8 m/s with the mass loss reaching 7.21 mm/year, these results can be seen in Fig. 15. Micro-cutting and local sand indentations are the major damaged mechanisms noted resulting is the surface roughness increasing.

Erosion and corrosion are usually found operating in tandem and is termed erosion-corrosion or tribocorrosion. Flow Accelerated Corrosion (FAC) and Erosion-Corrosion tests were conducted. Optical Microscopy (OM) was used to evaluate the different impact these degradation mechanisms had on the material surface. Fig. 16 showcases these results with a,b,e,f showing the effect of FAC and c,d,g,h showing erosion-corrosion. The effect of the interaction is clear with more corrosive products being removed when erodent's are present.

Erosion-corrosion tests were conducted at different velocities and a breakdown of the contributions from erosion enhanced corrosion and corrosion enhanced erosion were calculated these can be seen in Fig. 17c-d. Tests were also conducted looking at only corrosion over time which can be seen in Fig. 17a. When looking at lower velocities corrosion is the dominant mass loss contributor. As the velocities increase the impact of erosion becomes more prevalent but it is not until velocities increase to 8 m/s that it becomes dominant, as shown by the result in Fig. 17b-d. Between 3–8 m/s pitting is the main damage feature with these becoming stable after corrosion products are dispersed into them. This leads to retardation of erosion in the bottom of the pits with mainly corrosion contribution to further depth damage. Erosion and corrosion work together to increase pitting boundaries [40]. This mechanism is seen as an issue for oil and gas due to erosion-corrosion being present in extraction slurries containing acidic and oxygenated fluids with sand particles and has led to investigations into this interaction within pipelines.

Wang et al. investigated the effects of erosion and tensile stress on X70 pipeline steel when in a corrosive environment. They tested samples in a loop flow system to better simulate the real pipeline environment. Computer Fluid Dynamics (CFD) and electrochemical testing was carried out and found that both tensile stress and erosion would encourage general corrosion. In terms of localised corrosion, erosion is shown to be beneficial as it removes cations from pits slowing down the pit growth and breaking the cover of pits to stop them from developing into stable pits. On the other hand, tensile stress promotes localised corrosion due to reducing protective corrosion products and improve the reactivity of the steel [41].

Shahali et al. investigated the erosion-corrosion resistance properties of Sanicro28, a common material for the oil & gas industry due to its excellent corrosion resistance. Tests were performed at 4,5,6,7.5,9 m/s velocities using an erosive-corrosive slurry solution of 3.5 % NaCl saline water and 30 g/l SiO2 erodent particles. Tests were carried out at both 40° and 90° impact angles. It was found that the impact from particles led to corrosion rates increasing by up to 1000 times that of stagnant corrosion. The impact angle of 40° resulted in the most wear and it was found that as velocity increases with erosion, corrosion and erosion-corrosion effects also increase, this is illustrated in Fig. 18 were it can be seen that mass loss increases for both 40° and 90° but more so 40°. Looking at the synergy of erosion and corrosion it was observed that corrosion has a larger impact on erosion than erosion has on corrosion. The highest erosion-corrosion rate was 88±0.8 mg/cm^2.h at 40°, 9 m/s while the lowest was found to be 1.8 ± 0.3 mg/cm^2.h at 90°, 4 m/s [42].

The review of the existing studies in the literature shows that little research has been done to analyse the effects of erosion on AM built materials. This can be an opportunity for further application of AM in offshore renewable energy sector given the potential to create erosion resistance materials is made possible through increases in the material hardness and tuning of material properties. Erosion will be a key area of investigation to prolong tidal turbines and increase lifecycles of offshore renewable energy structures. Further interest in the renewable energy sector to combat corrosion-erosion may rise within offshore green hydrogen industry for the processing of seawater.

AM potentials for fatigue resistance

Offshore renewable structures undergo substantial amount of cyclic

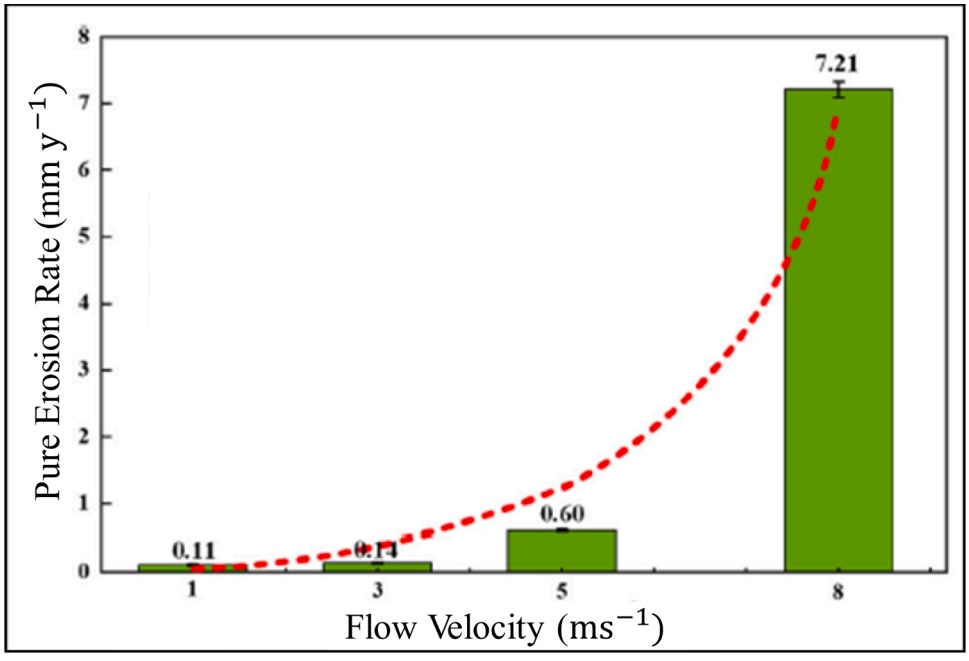

Fig. 15. The general pure erosion rate of EH 32 steels at different flow velocities. The general pure rate is fitted from the pure erosion equation and the fitting results are presented as the dashed line in the figure. The error bars represent standard deviations of the three repeated tests at each flow velocity. [40].

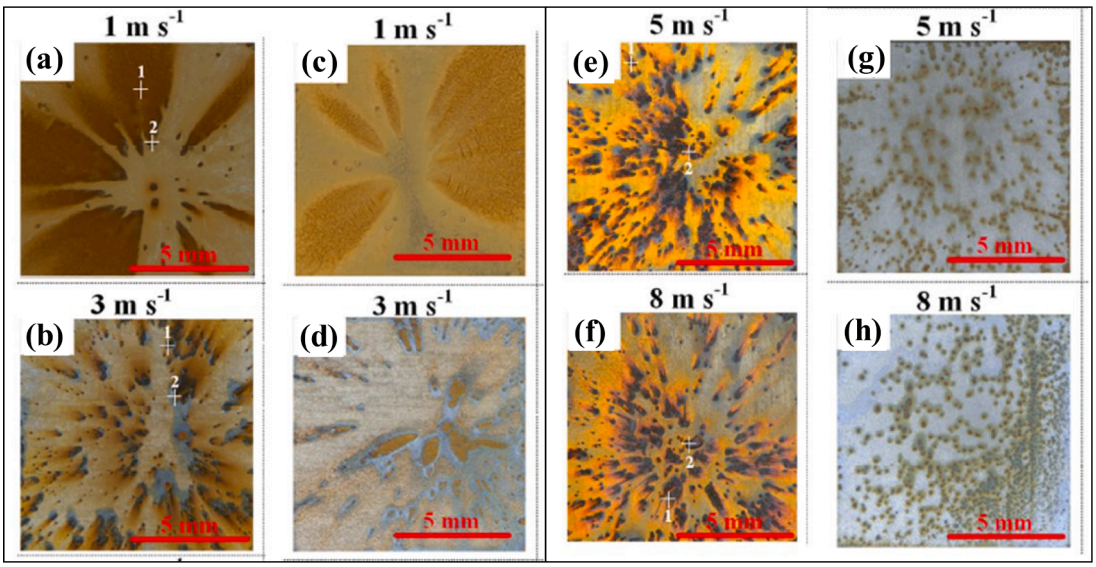

Fig. 16. Surface morphologies of the steel samples after tested in pure natural seawater: at 1 m/s (a), 3 m/s (b), 5 m/s (e), 8 m/s (f). and in natural sea water and erosion: 1 m/s (c), 3 m/s (d), 5 m/s (g), 8 m/s (h) [40].

loading from wind, wave, tidal and vibration loadings. This combined with surface degradation due to the marine environment leads to fatigue being a significant life limiting factor for the structures. Shamir et al. studied the effect of corrosion pits on the fatigue life of monopile weldments and found that as exposure time to a corrosive environment increases the fatigue life decreases drastically, this is detailed in Fig. 19 where it can be seen that as exposure time increases cycles to failure decrease [43].

Papatheocharis et al. compared welding technologies and post treatments for welded X joints for OWT jackets as the geometry of these joints leads to hot spots which in turn enables fatigue damage. From this it was shown that manual welds have the lowest fatigue life when compared to automatic welding. By conducting High Frequency Mechanical Impact (HFMI) the fatigue resistance was also greatly improved, as shown in Fig. 20 were hammer peening has the best fatigue resistance and mannuel generally has the worst [44]. Chatziioannou et al. have further expanded on this work looking at high strength steels S420 and S700 for the use in X joints for improved fatigue resistance against Ultra Low Cycle Fatigue. They found that the fatigue performance of S420 and S700 is like that of mild steel [45].

Due to the lack of significant number of installed floating OWT there is a gap in the fatigue performance of such structures. However, learning from the experience of onshore and fixed bottom wind turbines, it is suspected that due to the aerodynamic and hydrodynamic loading on these large structures fatigue will be also an issue. López-Queja et al. conducted a review of the control strategies of floating OWTs and found that many modelling techniques have shown that fatigue life can be extended if adequate control strategies are employed to reduce aerodynamic and hydrodynamic loading [46]. Ramezani et al. conducted a review on the uncertainties of fatigue reliability modelling and found that wave characteristics have a larger impact on floating OWT compared to fixed bottom structures. Cycle-dependant fatigue damage uncertainties were highlighted as being continually growing over time of operation. However, in practices these are not accounted for in the analysis of fatigue reliability and showcase a lack of knowledge of these areas [47]. Zou et al. reviewed literature to highlight the impact of manufacturing imperfections that can affect the fatigue life of offshore renewable energy structures. The three main imperfections detailed were, flatness divergence of flanged connections, loosing of bolted connections and tilt angle of the tower. Flange divergence arises from the geometric constraints on the flanges and tolerance margins. Bolted connections were seen to loosen from the installation vibration and in turn increase cyclic stress range. Tower tilt angles from fixed turbine were noted to be redundant for floating OWT because of higher motions due to the environment [48]. These studies highlight a large lack of knowledge in terms of cyclic loading and fatigue effects on floating OWTs performance but do highlight that there are expected to be larger than that of fixed bottom wind turbines. The designs and manufacturing of floating OWTs greatly impact the fatigue of the system and should be well understood before construction and installation.

TEC fatigue knowledge gap is even bigger than that of floating OWTs in terms of structures. TEC fatigue generally is concerned with the blades and effects of loading on the fatigue life of structure is very limited. However, one study carried out by Mullings et al. looked at the fatigue loading on tidal structures in terms of Damage Equivalent Loads (DEL) using data from the European Marine Energy Centre (EMEC) in Orkney, Scotland. Two locations were analysed at both near surface and near bed. The results showcased the trend that near bed has higher loading than that of near surface. Location variations were highlighted with the two sites having a variation on 28 % for near bed and 41 % for near surface values [49]. The lack of literature reflects the lack of knowledge in long-term fatigue of TEC systems. Unlike floating OWTs, TECs do not have a similar technology in which to take lessons learned from.

WECs, like wind and tidal, experience the fatigue due to the loading nature offshore. Papatheocharis et al. carried out fatigue and mechanical testing for an Oscillating Water Column (OWC), a type of WEC, design that was to be coupled with a floating OWT. They completed a fatigue assessment on 10 welded tubular joints from the buoyancy section. These tests have revealed locations of expected failure, which is always in the weld toe at the crown of the brace-to-cylinder backing up the numerical modelling. This failure location can be seen in Fig. 21 were after 4060 cycles at 90 kN it failed. High-frequency mechanical impact (HFMI) was applied to the welds to assess if this post treatment would increase the fatigue life. The results showed that in high-cyclic fatigue this did but in low-cycle no obvious change is seen [50]. Shahroozi et al. created a simulation using WEC-SIM of a shackling on a Point Absorber, another type of WEC. A linear relationship between fatigue equivalent loading and maximum force was noted for the different sea states. Based on a 50-year return wave the total equivalent force was 2.42MN for 2×10^6 cycles [51].

WAAM is seen as a promising AM process for creating components for the offshore environment and as a result has seen research into the performance of WAAM materials. Ermakova et al. investigated the fatigue resistance of ER100S-1 in multi-axial, uniaxial and torsion then

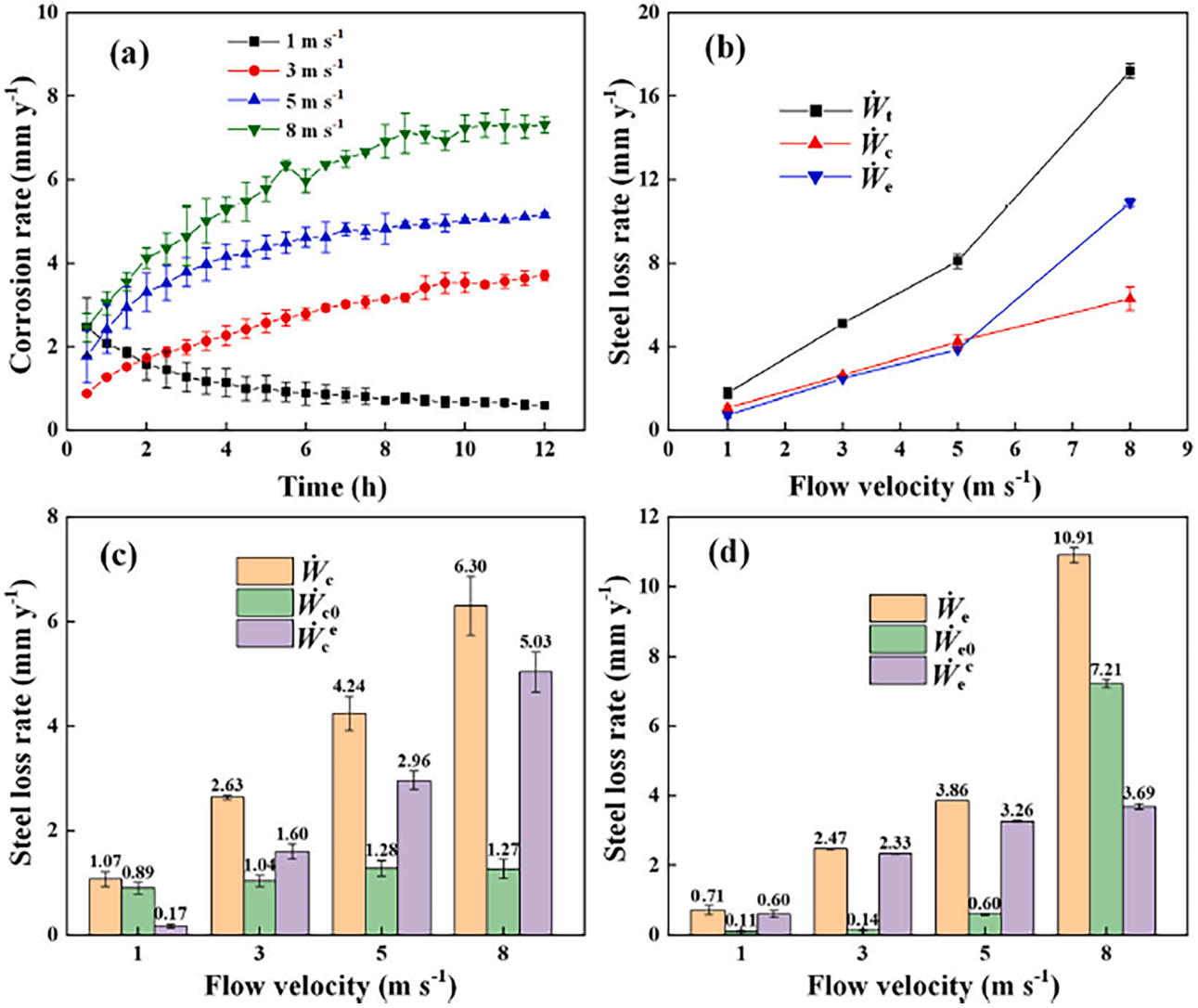

Fig. 17. The measurement and the calculation results of the erosion−corrosion at different flow velocities. (a) Time dependence of the instant corrosion rates. (b) The total steel loss rate, general corrosion rate, and erosion rate. (c) The general corrosion rate, pure corrosion rate, and erosion enhanced corrosion rate. (d) The general erosion rate, pure erosion rate, and corrosion enhance erosion rate. The error bars represent standard deviations of the three repeated tests at each flow velocity. [40].

compared these results with other steels. Uniaxial testing yielded the best fatigue results followed by torsion at 22.2 % lower and multi-axial at 45.8 % lower than uniaxial. Compared to other steels, including S355 commonly used in offshore structures, ER100S-1 proved to provide the best performance [52]. Fig. 22 illustrates this to be the case comparing a variety of different steel grades to ER100S-1 in a-c as well as a comparison to the design standard DNV C1.

Ermakova et al. also looked at the fatigue crack growth behaviour of ER70S-6 and found that it falls beneath the recommended crack growth rates of BS7910. However, the material has higher fatigue crack growth rates than HAZ S355 and is comparable with S355G8+*M* base metal [53]. Webster et al. carried out a study looking at ER100S-G for the use in submarines. They compared ER100S-G to ER70S-6 and ER100S-1 showing that in terms of fatigue life it is better than ER70S-6 and worse than ER100S-1 [54]. Ayan et al. has carried out an investigation on the fatigue life of ER70S-6. From this a fatigue life over x10^7 cycles was obtained at a stress of 178 MPa for vertical and 176 MPa for horizontal. These results are comparable with ST37 [55]. Huang et al. completed a total on 75 fatigue tests on ER70S-6 with and without machined surfaces. They found that un-machined surface samples resulted in a 35 % reduction in fatigue life, as shown in the S-N curve in Fig. 23, when compared to machined. The machined surface samples are comparable to S355 in terms of fatigue life and show a similar S-N trend [56].

Huang also analysed ER70S-6 and ER110S-G for fatigue crack growth behaviour and compared these against conventional hot rolled steels. The WAAM specimens showed similar values to that of conventional steels. Higher strength WAAM steel (ER110S-G) showed a greater fatigue crack growth resistance to that for ER70S-6. Results showed good agreement with BS7910 for unwelded steel fatigue crack growth rates. He et al. compared ER70S-6 vs hot rolled Q2325 steel in terms of fatigue life and fatigue crack growth, which was measured via in-situ Acoustic Emission (AE) measurements. ER70S-1 was shown to have better fatigue life and more resistance to fatigue crack growth than that of Q235. AE from the samples showed different trends, with the AE from Q235 having 70 % of the activity occurring before main crack occurs and WAAM had the majority for activity during crack propagation [57]. Ron et al. has investigated the effect of corrosion fatigue on ER70S-6 and ST-37. From their findings it was discovered that both materials have similar fatigue lives in air. However, in a 3.5 % NaCl solution the ER70S-6 has considerable reduction to 140 MPa whereas the ST-37 had fatigue strength of 240 MPa. This was deemed to be due to

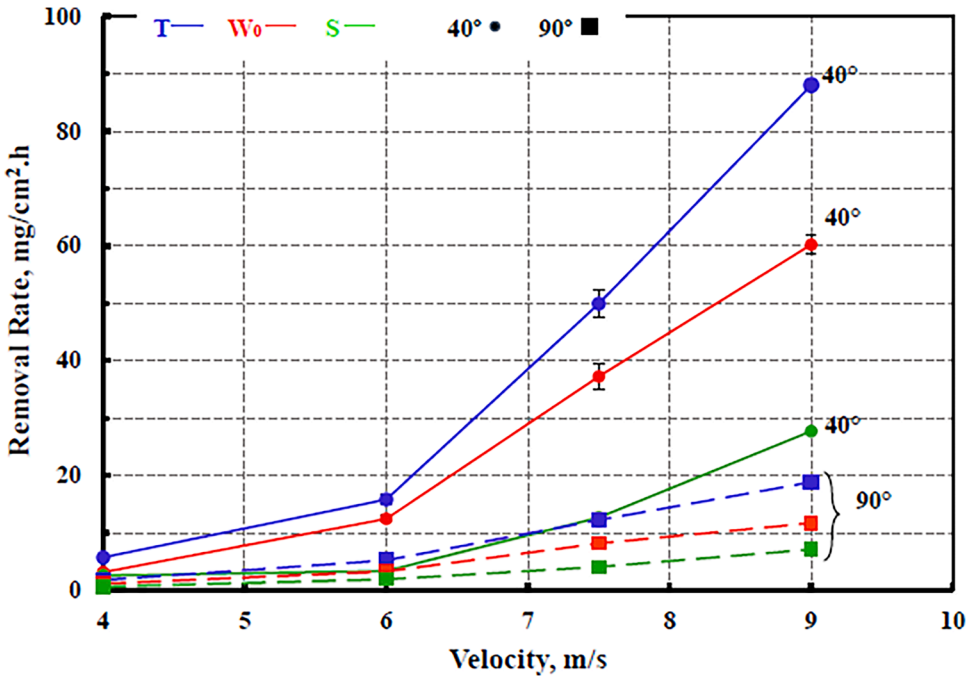

Fig. 18. Effect of impact velocity on the erosion-corrosion (T), pure erosion (W_o) and synergy (S) rates of Sanicro28 stainless steel in 3.5 wt% NaCl slurry containing 30 g/l SiO_2 under impingement angles of 40 and 90° [42].

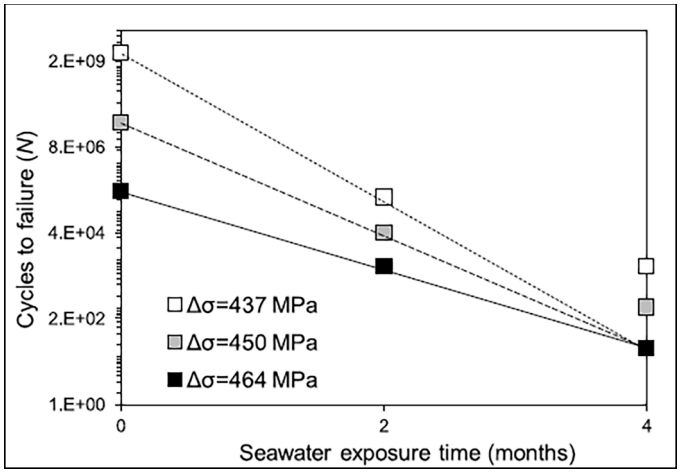

Fig. 19. Correlation of number of cycles to failure (N) with seawater exposure time at multiple stress levels [43].

manufacturing defects such as porosity, lack of fusion and impurities which were areas that attracted corrosion [58]. Ji et al. looked at the effects of using WAAM with in-situ ultrasound on the melt pool. The purpose was to see the effects on the microstructure and to reduce columnar grains and create equiaxed grains throughout the material. Columnar grains are an issue in WAAM as they can make the material anisotropic resulting in a reduced fatigue life and strength compared to the same material with equiaxed grains. Three ultrasound scenarios where investigated: 0 μm, 4 μm, and 12 μm of ultrasonic input amplitude. The results concluded that 12 μm amplitude yielded the best results and effectively ensured equiaxed grains were formed. This can clearly be seen Fig. 24, that present OM images generated after grinding and polishing, a1–2 show the microstructure before ultrasonic treatment and b1–2 show how it has changed after 12 μm input [59].

Fatigue-Corrosion-Erosion interaction

The offshore environment is very hostile requiring the implementation of rigorous requirements for offshore systems. As previously noted, fatigue along with corrosion and erosion can affect the life of offshore structures. Erosion and corrosion have a complex relationship where they can influence one another. Fatigue can influence corrosion due to the breakage of passive films in passive steels encouraging pitting. The interaction between the three mechanisms is rarely looked at as a whole system and instead corrosion-erosion, corrosion-fatigue or erosion-fatigue interactions are investigated. This interaction of fatigue-erosion-corrosion has been seen in the first generation of drilling platforms, which seen their hydraulic cylinders for riser tensioners fail at a higher-than-expected rate due to the combination of wear-corrosion-fatigue mechanisms leading to greater surface damage than expected. With offshore renewables being a high paced, high demand product to market environment lessons from oil and gas should be considered to avoid delay in technology development. Von der Ohe et al. carried out an investigation to create a multi-degradation model for these hydraulic cylinders and created an expression on which to calculate the material from the interaction of corrosion, wear, embrittlement and loading. They found that wear-fatigue interaction led to the decrease of fatigue life by a factor of 2 for medium carbon steel UNS G10450. They also highlighted that although higher hardness leads to an increase in the resistance to multi-degradation; surface elasticity and toughness can be just as critical in increasing resistance to wear from abrasion, erosion and impacts [60]. This leads to the need for materials to be finely tuned in terms of hardness and elasticity to provide the best resistance to their environment and application.

WAAM has shown it can manufacture materials with mechanical and fatigue properties equal to or greater than that of the wrought material. Manufacture of corrosion resistance materials has also been proven possible via WAAM. Due to the nature of the process WAAM has the potential to alter the material properties of a part via mixing materials in the melt pool or adding processes to enhance the microstructure. This raises the question of can additive manufacturing be used to create a material that is optimised for combatting the interaction of fatigue-erosion-corrosion, an interaction which is detailed in Fig. 25. By

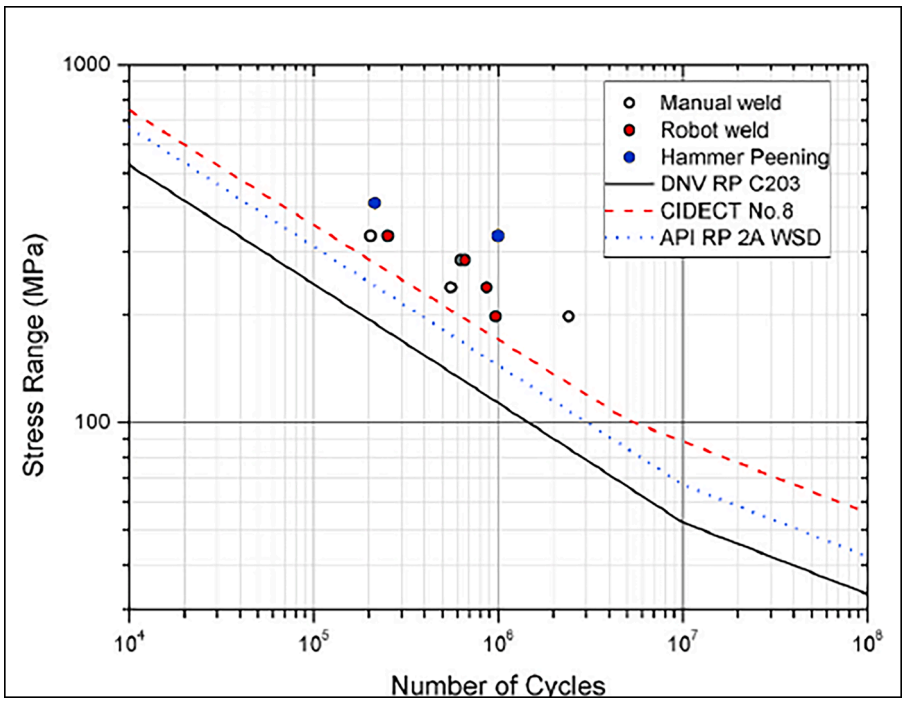

Fig. 20. Fatigue results for manual welding, robotic welding and hammer peening against design standards [44].

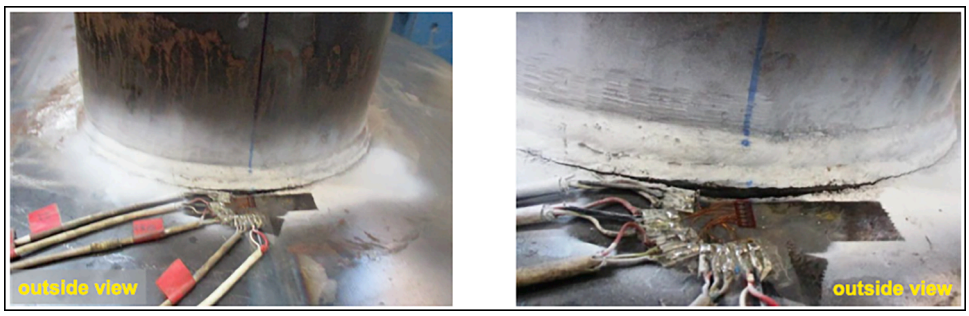

Fig. 21. Through-Thickness Fatigue crack development for WTJ-7 after 4060 at $P = 90$ kN [50].

optimising for these mechanisms offshore renewable energy structures can implement AM components that will be able to either extend the life of existing infrastructure or help design structures that will be capable of lasting longer than the current 20–30 year life expectancy.

Advantages of multi-material AM build strategies

The previous studies of AM presented and discussed above all look at single material builds. However, AM can create multi-material components with in-situ mixing of materials. This gives an excellent opportunity to explore the possibility of tailoring materials to either a specific environment or application. In this section multi-materials and building strategies are discussed.

Functionally graded materials AM

Functionally Graded Materials (FGMs) are materials that are designed for specific applications with the joining of two or more materials. The purpose of this is to exploit the material properties of the two or more materials to meet the requirements of a component whilst keeping costs down. For example, a corrosive resistant material on the surface transitioning to a cheaper steel for the bulk material. They can either be a gradient or stepped transition from one material to other. AM is a great way to construct FGMs due to the layer-by-layer process. WAAM, due to the ability to print large parts, is ideal for the manufacturing of FGMs for the offshore industries. FGMs could be an excellent solution for optimising components to resist against the fatigue-erosion-corrosion interaction. Many works have been carried out analysing the properties of FGMs built from WAAM.

Gradient FGMs transition from one material to another via percentage change along the build height. Gradient composition gives the ability to have better control of how and where a material fails. Zhang et al. evaluated the composition gradient of IN625/HSLA FGM to carry out optimisation of the gradient layers, Fig. 26 shows the composition layer by layer for the wall. From this low strength regions such as 70 % HSLA steel- 30 % IN625 and 60 % HSLA steel-40 % IN625 were removed from the optimised FGM. Laves phases were also noted to be in high concentration in regions 30 % HSLA steel-70 % IN625 and 40 % HSLA steel-60 % IN625 which were stress concentration and ultimately lead to cracking initiation sites. These layers were also removed from the optimised material. Tensile tests were conducted at room temperature and 700 °C. The optimised material improved from 449 MPa to 509 MPa at room temperature and 403 MPa to 464 MPa at 700 °C. This optimisation meant areas of high stress concentration and fracture were moved to a more desirable position giving more control over the materials properties. Fig. 27 shows the stress-strain results for before and after

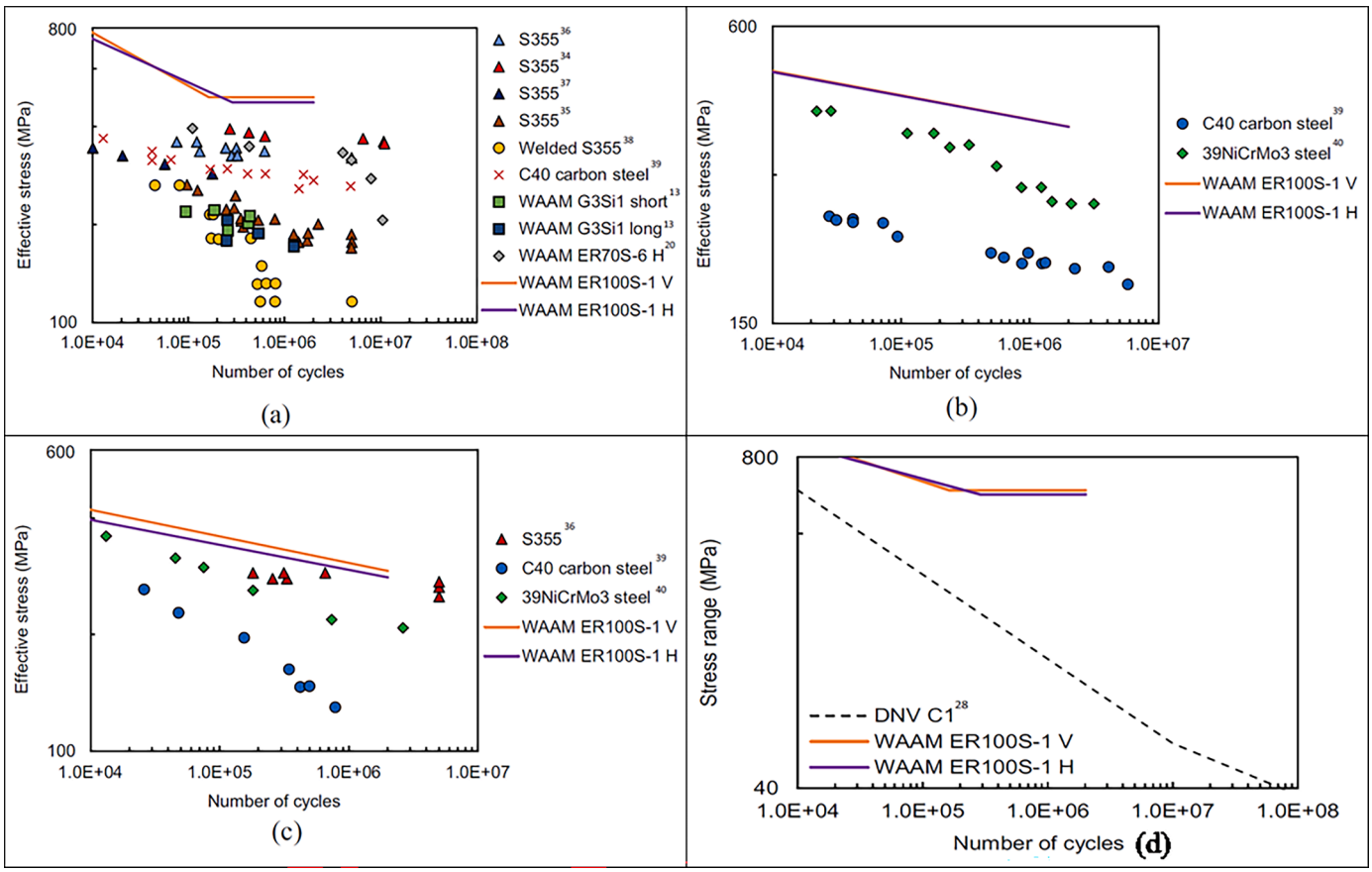

Fig. 22. Comparison of fatigue data for WAAM ER100S-1 with data in the literature for (a) uniaxial, (b) torsion, and (c) multi-axial fatigue tests on steel and (d) with DNV C1 recommended design curve [52].

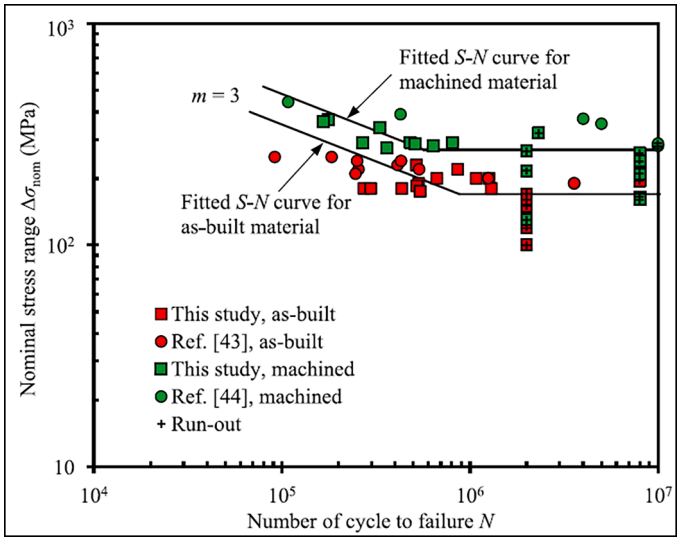

Fig. 23. Comparison of fatigue test results of as built and machined WAAM coupons [56].

optimisation along with Digital Image Correlation (DIC) images illustrates how the stress concentrations have moved position [61].

Stepped FGMs are more commonly researched for WAAM and is the transition of 100wt% of one material to 100wt% of another. This method produces an interface region where the two materials fuse together [62]. Ayan et al. created an FGM of ER70S-6 and 308LSi into an alternating layer by layer construction [63]. This was then tested for mechanical and fatigue properties. The material showed an alternating hardness value through the layers from 226HV in 308LSi layers to 370HV in ER70S-6 layers. This created an FGM where each layer was alternating from ductile to brittle, as demonstrated in Fig. 28 where the failure location is also shown. Tensile tests showed an average of 709 MPa in the vertical and 740 MPa in the horizontal specimens. Greater variation was noted in the horizontal due to the different layer combinations. These values are 46 % higher compared to low alloy steel and 40 % than stainless steel showcasing the benefits to mechanical properties FGMs can offer. The fatigue limit for the specimens showed good performance. However, it should be noted that the horizontal specimens had a 25 % higher fatigue life and therefore orientation of components to layers should be considered in design stages of parts [62, 63].

Ayan et al. similarly investigated a stepped FGM of ER70S-6 and 308LSi with only one interface between the layers, this can be seen in Fig. 29 where the composition step it detailled. From this it was found that the tensile tests gave the same material strength of the material in that region with the ER70S-6 average being 484 MPa and 532 MPa on the 308LSi side. However, the strength of the material at the interface was 544 MPa and is the highest strength region. Horizontal specimens gave higher strength than that of the vertical as the vertical specimens always failed on the ER70S-6 section. A fatigue limit of 170 MPa was calculated, and some samples were found to be intact after x10^7 cycles [62,63].

These results are similar to that of Chandrasekaran et al. which explored using a FGM of ER70S-6/ER2209 for the application of marine riser in the oil and gas industry. This carbon manganese/Super Duplex Stainless Steel material underwent X-ray inspect for defects in which only slight lack of fusion was noted. Tensile testing was conducted for

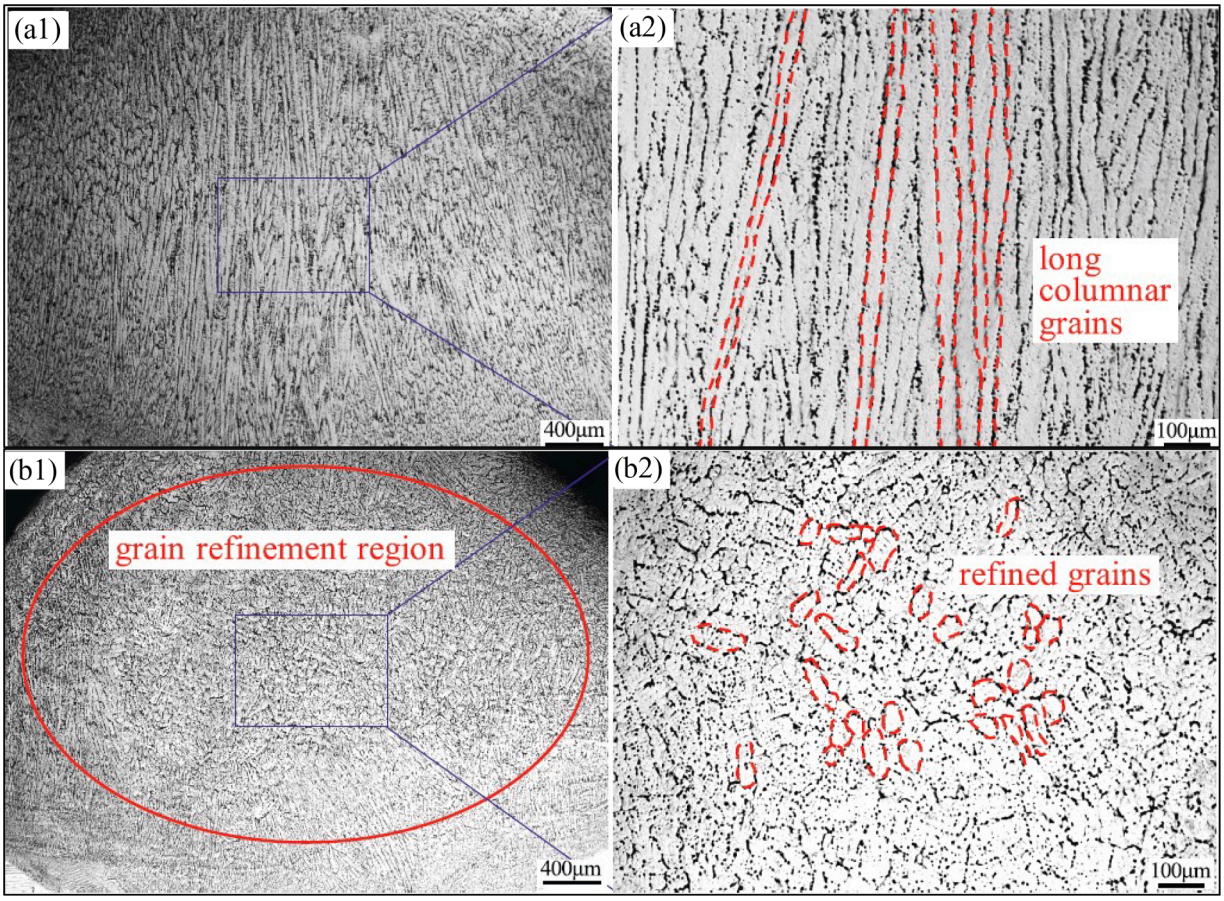

Fig. 24. (a1–2) WAAM microstructure before addition of ultrasound, (b1–2) After 12 μm of ultrasound during manufacture [59].

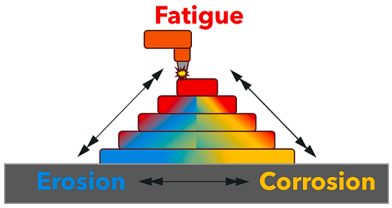

Fig. 25. Interaction Concept for Fatigue-Erosion-Corrosion.

the samples in the vertical direction giving a Yield Strength (YS) of 360 MPa, Ultimate Tensile Strength (UTS) of 485 MPa and an elongation of 16 %. Failure occurred in the ER70S-6 region and fractography revealed the presence of dimples indicating ductile fracture. Compared to X-52, a common oil and gas steel, the yield and elongation was lower. However, the UTS was 6 % higher [64]. Kumar et al. analysed SS321/Inconel 625 FGM in terms of mechanical and microstructure properties. Tensile test results showed that the SS321 section had higher strength than that of its wrought material. Whereas the Inconel section had comparable strength to its wrought material. The interface had a greater strength than that of the SS321 but not of the Inconel. The fracture always occurred in the SS321 section of the material [65]. Sasikumar et al. created a FGM of SS316L/IN625 using ER316L/ER625 and examined its mechanical and microstructural properties. Tensile results showed that at the interface in the horizontal direction the YS was 448 MPa, with an UTS of 804 MPa and an elongation of 25 %. In the vertical direction the interface gave an YS of 531 MPa, an UTS of 845 MPa and an elongation of 19 %. The YS and UTS was between that of the SS316L and IN625 but the elongation was lower than both materials in all cases. The present of laves phase in IN625 and δ-ferrite has

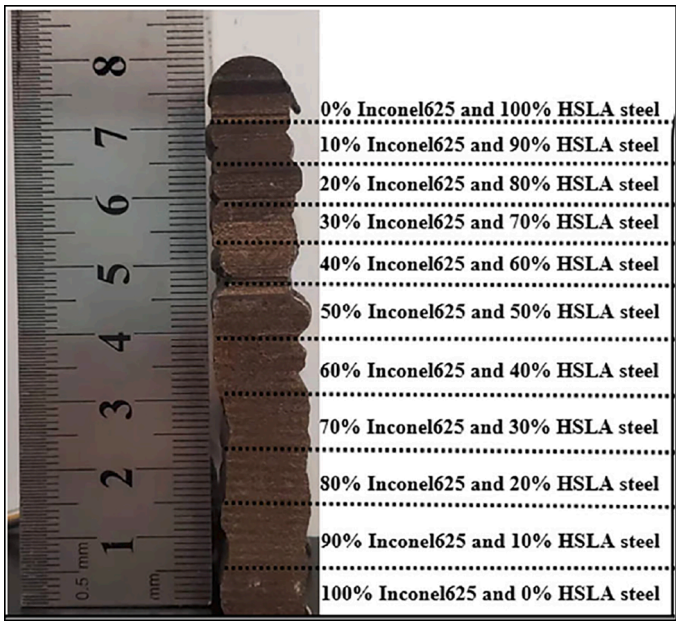

Fig. 26. Gradient FGM of IN625/HSLA [61].

significantly influenced the properties of the material. These laves phase can be seen in Fig. 30 which are microscopic images of the material at different locations along with build height; after being electrolytically etched with a 50/50 mix of nitric-acid and distilled water for 15 s as per ASTM E3-11. All samples failed via ductile failure mode and SEM

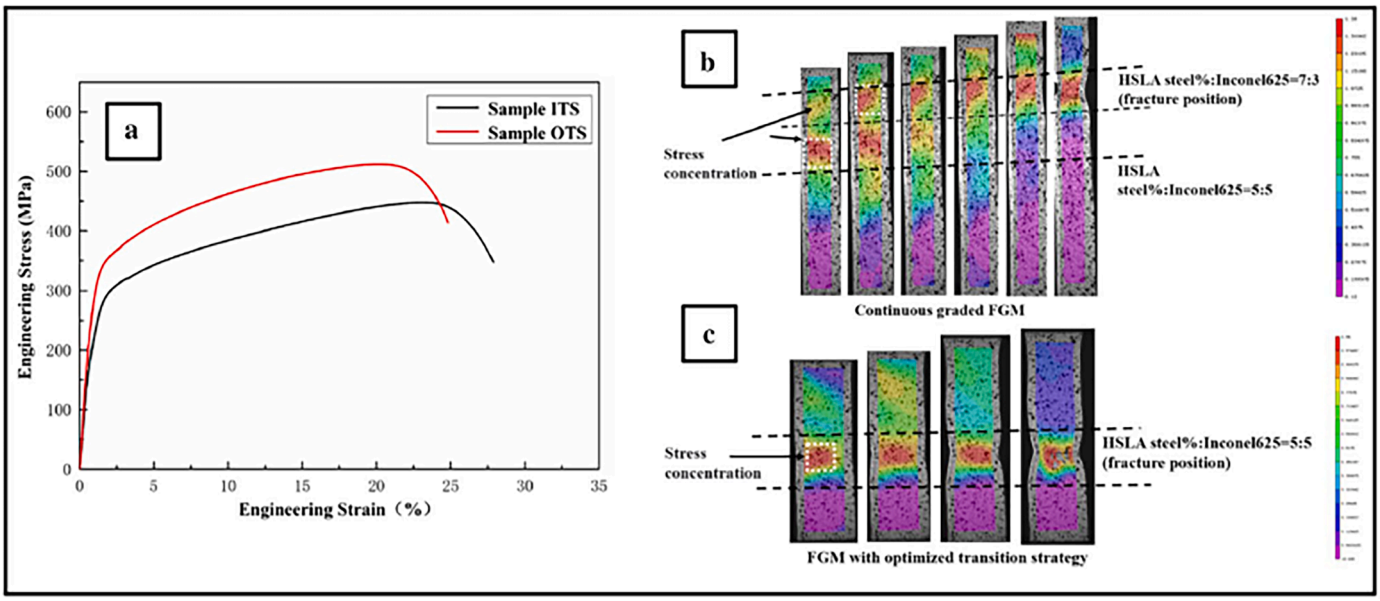

Fig. 27. Mechanical properties of the FGMs: an Engineering Stress-Strain Curve, b DIC test of sample OTS [61].

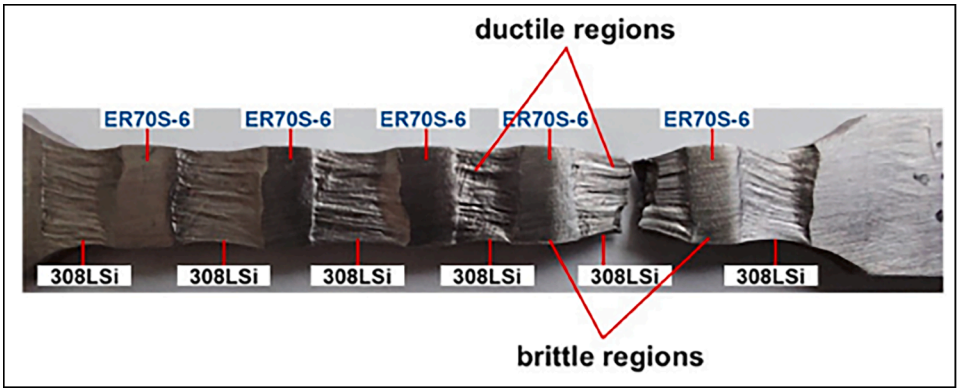

Fig. 28. Marco Image of the Vertical Tensile Test Specimens [63].

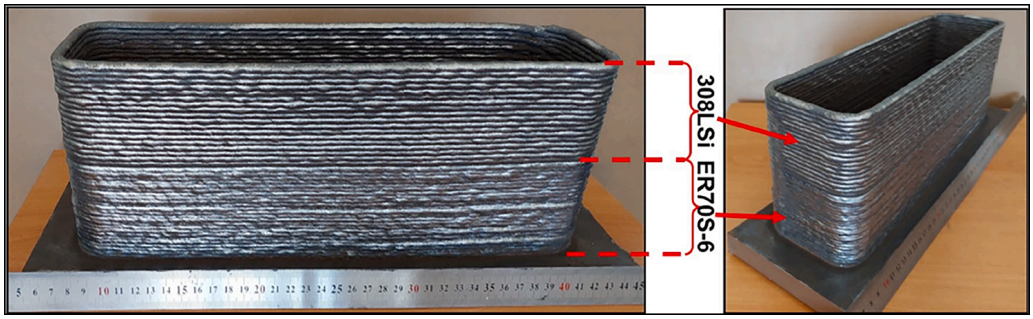

Fig. 29. Stepped FGM of ER70S-6/308LSi Test Wall [63].

revealed dimples in the SS316L and interface regions. In the IN625 regions dimples and voids were noted [66].

Rajsh Kannan et al. explored the tensile and fatigue properties of SS904L/Hastelloy C-276 FGM. A wall was built with SS904L transitioning to Hastelloy via an interface region. Test specimens only looked at the vertical orientation with the interface region in the middle of the samples. From tensile tests all samples failed in the SS904L region with an average YS of 311.08 ± 9 MPa, UTS of 680.73±12 MPa and elongation of 37.87 ± 2.5 %. These properties are greater than that of the wrought material. The FGM reached 2×10^6 cycles at 156 MPa, as shown in S-N graph in Fig. 31 which details the testing results and shows sample specifications. However, the fatigue life of the samples was 28–35 % less than the fatigue life of SS904L wrought. The fracture surface demonstrated the ductile fracture characteristics [67]. Rodrigues et al. successfully manufactured a HSLA/Cu-Al FGM via Twin-wire and Arc Additive Manufacturing (T-WAAM). From their assessment of the material, they found that the process of remelting and heating led to a large interface region of ≈12 mm. The UTS of the material was found

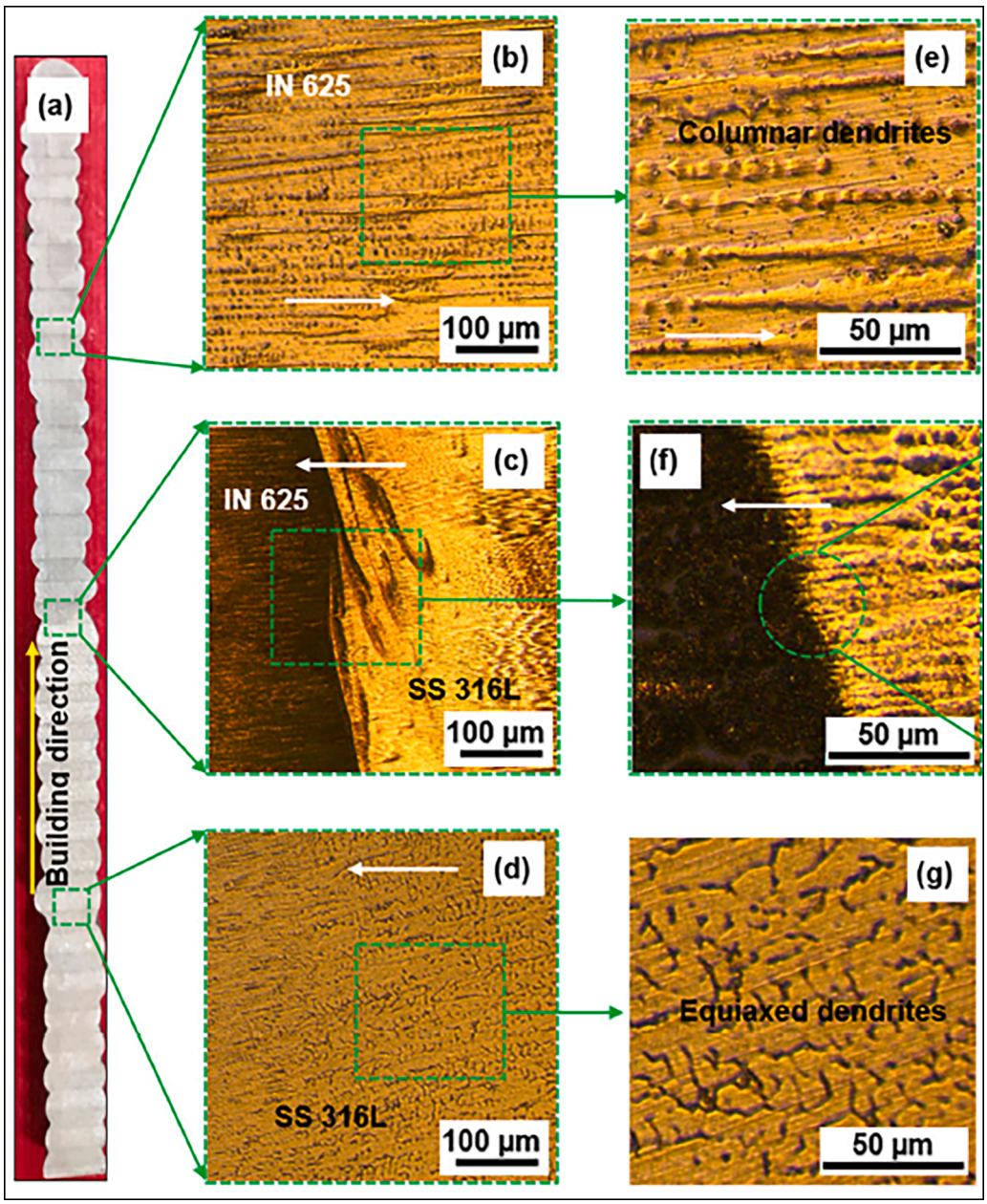

Fig. 30. Micrographs of the WAAM processed FGM at various regions: (a) macrograph, (b and e) microstructure at IN625, (c and f) interface region, (d and g) [66].

to be 690 MPa and is higher than that of Cu-Al but lower than HSLA. The elongation was 16.6 % and lower than both base materials. The reason for this in down to the microstructure created at the interface where dendritic-type Fe phases and β precipitates in the Cu matrix are present. On the fracture surface dimples and cleavage facets were present. As a result, the fracture was deemed to be a mixture of ductile-like and quasi-cleavage type fracture [68].

All these studies successfully manufactured FGMs of different materials. A common theme is that the FGM meets or exceeds the mechanical properties of the lower strength wrought material. Most experiments have been conducted in the vertical direction where failure is always in the lowest strength material region. The horizontal samples show that the interface can could provide better mechanical properties in this direction, but more research is required and therefore highlights a current gap in the knowledge.

All of these studies underwent hardness testing along the build height. Ayan et al. FGM of ER70S-6 and 308LSi found that hardness values at the interface are the highest hardness values for the material [63]. Chandrasekaran et al. FGM of ER70S-6/ER2209 discovered that the microstructure of the interface was martensite formed in the carbon manganese steel due to the diffusion of alloying elements from the SDSS, this can be seen in Fig. 32 where the area near the interface is shown. These images were captured via OM after undergoing polishing from different grades of emery paper and diamond paste before being electrolytic etched using 10 %NaOH and 4 % Nital. This disffusion led to high hardness values at the interface of the two materials in the range of 307–320HV, which can be seen from Fig. 33 that details the hardness values throughout the build height of the wall. Kumar's et al. FGM of SS321/IN625 also found the hardness of the material to be at its highest at the interface. However, Sasikumar et al. FGM of SS316L/IN625 presented hardness measurements with an average hardness of 168, 198–214 and 227HV in the SS316L, interface and IN625 areas respectively. Rodrigues et al. FGM of HSLA/Cu-Al the failure location for the samples occurs in the copper region near the interface region. This demonstrates the higher hardness levels at the interface compared to the Cu-Al. These two studies show that the interface is not the hardness but

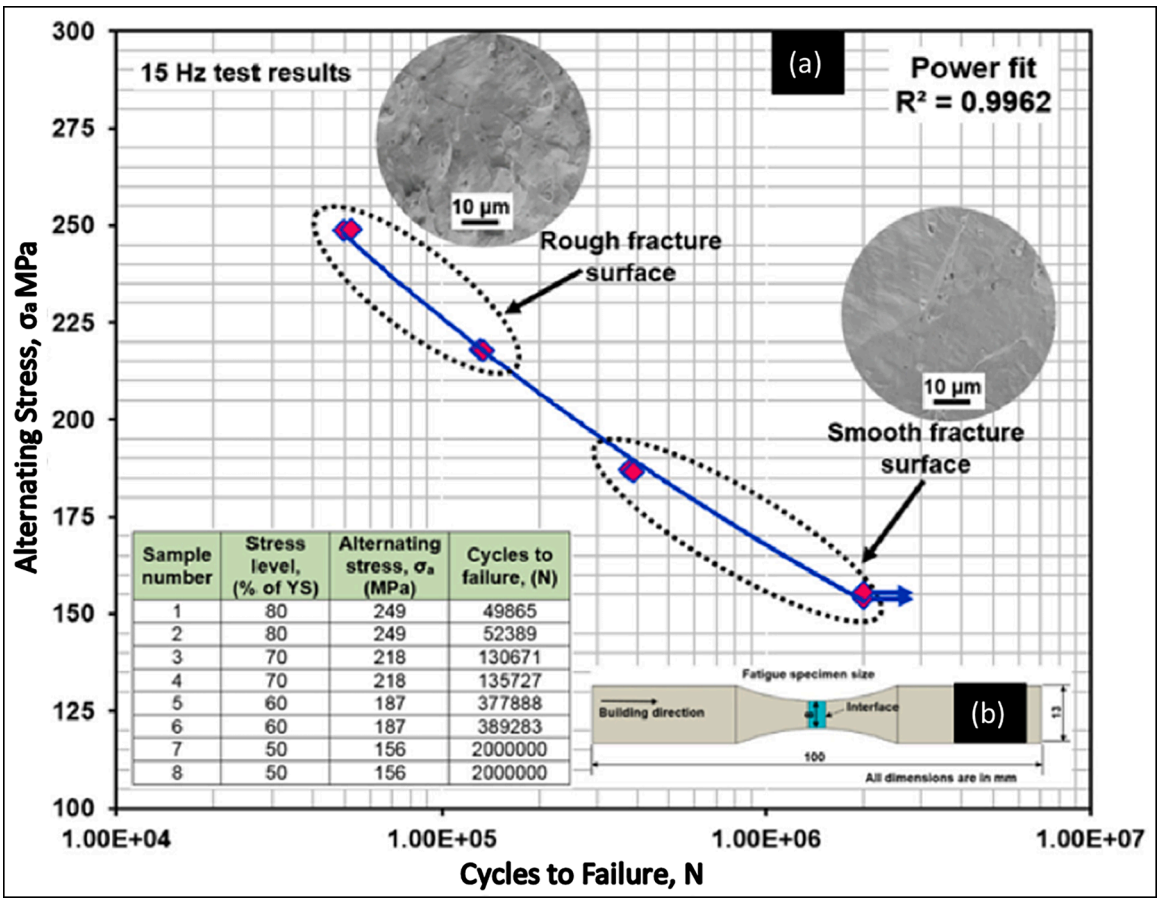

Sample number	Stress level, (% of YS)	Alternating stress, σ_a (MPa)	Cycles to failure, (N)
1	80	249	49865
2	80	249	52389
3	70	218	130671
4	70	218	135727
5	60	187	377888
6	60	187	389283
7	50	156	2000000
8	50	156	2000000

Fig. 31. (a) S-N curve and (b) fatigue specimen size [67].

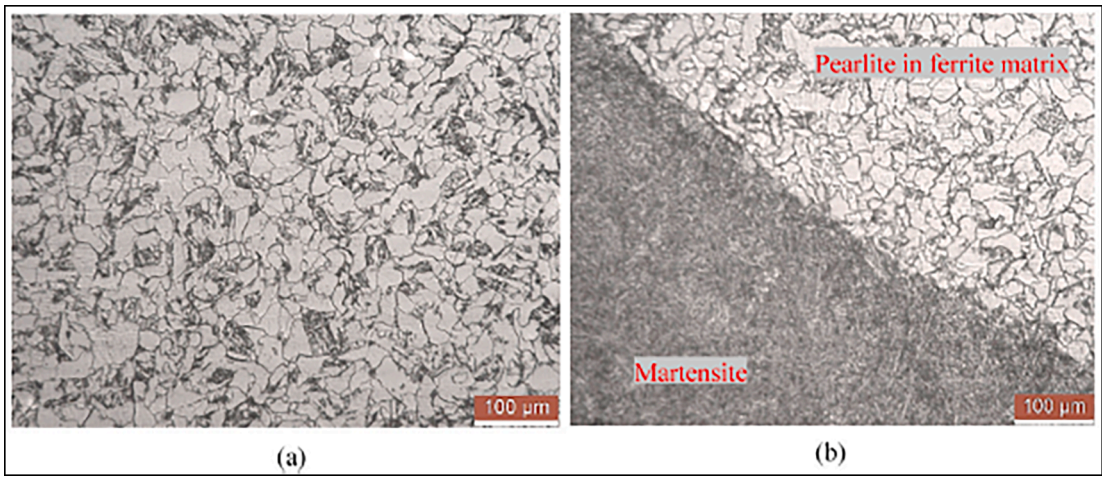

Fig. 32. Microstructure of carbon-manganese steel obtained from an optical microscope from near interface region. [64].

is harder than that of the lower strength material. This raises the questions of what the material behaviour trends are for different combinations and how can they be optimised for applications.

Little comparison has been made between gradient and stepped strategies in terms of properties. Rodrigues et al. investigated the gradient and stepped transition strategies of 316 L/IN625 FGM and how they impact the mechanical performance. When looking at the stepped sample it was found that no defects or thermal cracking was present at the interface region. The microstructure presented a sudden change in grain structure from one material to another and γ'' phase could have been present in the IN625 region due to enrichment of Nb. In the gradient sample precipitates were noted across the compositional region. From Energy-dispersive X-ray spectroscopy (EDS), interdendritic areas were analysed and segregation of Nb and Mo in these indicate the presence of laves phase and carbides. Residual stresses were measured via neutron diffraction on both samples, and it was found that the stepped sample had compressive stresses in x, y, z with up to 180 MPa in the z, as demonstrated in Fig. 34 that illustrates the residual stresses throughout the build height for both FGMs. The gradient sample had considerably higher residual stresses with the 55 wt.% IN625 region

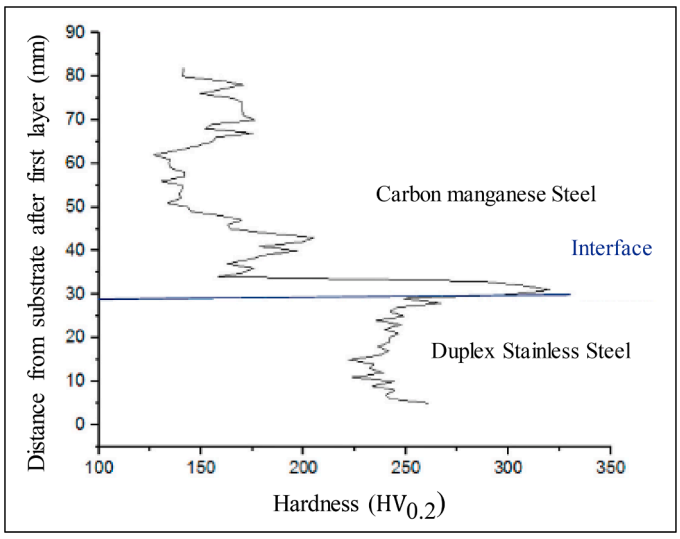

Fig. 33. Variation in micro-hardness along with the functionally graded build [64].

giving tensile stresses of 314, 348 and 468 MPa in x, y, z. These high residual stresses were suspected to be due to the present of δ-phase (Ni3Nb), σ-phase, and carbides. The hardness of both materials was measured and found that the hardness was high in the first layers at around 200HV before dropping to about 173HV after 35–40 % build height. This is due to the fast-cooling rates and high carbon content of the substrate. After dropping the values steadily climb until the maximum value of 220 HV at the 80 % total height in the IN625 region. From UTS and elongation tests the stepped sample performed better than the gradient sample with values of 542 MPa, 61.6 % and 503 MPa, 32.4 % respectively. The decreased tensile properties of the gradient material were deemed to be a result of the different phases present in the material. The stepped samples all failed at the interface region whereas the gradient samples failed in the 65% wt. 316 L region. Fractography revealed that the stepped samples demonstrated ductile-like fractures due to a homogenously distribution of fine dimples. The gradient samples had a mixture of dimples and quasi-cleavage facets. However, the samples still had a high elongation before fracture [69].

Yu et al. studied the mechanical properties of FGM 316 L/IN635 with a gradient composition and stepped comparing the two. This was carried out using dual-wire plasma arc additive manufacturing (DW-PAAM) which allows for the materials to be mixed in the melt pool during manufacture and no defects were found in the transition zones. The microhardness of this showed that the gradient material had a higher microhardness and a more gradual increased compared to that of the stepped material, as shown in Fig. 35 which presents both FGMs hardness values throughout the build height. Tensile strength and elongation were very similar. However, the gradient material performed worst in terms of UTS and YS [70]. The lack of comparison for these two FGM strategies from WAAM in the literature shows a large knowledge gap that should be filled to enable the better design of FGM components.

Zhang et al. investigated how to improve the mechanical properties of FGMs via Electromagnetic Stirring (EMS) and Heat treatment. In both cases they analysis IN625/HSLA FGM. Their first improvement was using EMS during manufacture to reduce Laves phase within the material. This led to dendrite spacing reducing by 22.6 % and hence decreasing Laves phase sizing from 2 μm to less than 100 nm. This resulted in a change to the mechanical properties leading to an increased hardness, UTS and YS, this can be seen Fig. 36 where these properties are compared for the varients of without EMS, 3,4 and 6 Hz of stirring [71]. The next improvement was to introduce in-situ heat treatment as well to evaluate its impact on the mechanical properties of IN625/HSLA. This was done by heating the WAAM wall after the 50/50 % material mix layer for a 1-hour and 2-hour periods. Results from tensile tests showed that heat treatment improved the mechanical performance with the 1- and 2-hour treatments yielding values of 584 ± 10 MPa and to 602 ± 10 MPa respectively. This is up from the cold work wall that had a strength of 512 ± 15 MPa. The reason for the increased strength is deemed to be from the laves dissolution within the material and creating Nb-rich carbides precipitation [72].

There are very few articles on the corrosion performance of FGMs. However, Senthil et al. studied the corrosion performance of stepped SS316L/IN825 FGM. The testing involved submersing specimens from the SS316L, IN825 and interface regions in a 100 g of ferric chloride hexahydrate and 900 ml of distilled water solution. These were left at 50 °C for 24, 48 and 72 h. From this the results showed that the interface had the highest resistance followed by the IN825 and then the SS316L with material loss rate of 0.1087 g, 0.1349 g and 0.4620 g, respectively. This is deemed to be from the higher concentrations of NiO and Cr_2O_3 along with reductions in MoO_3 at this region. Spallation was observed on the SS316L and IN825 specimens, but little was observed on the interface sample [82].

Chandrasekaran et al. conducted pitting corrosion testing of the two regions in ER70S-6/ER2209 as per ASTM G48-11 in a test solution of 100 gm of reagent grade ferric chloride and 900 ml of distilled water. This resulted in corrosion rates of 70.77 and 823.35 g/m^2 for ER2209 and ER70S-6 respectively [64]. Pütz et al. analysed the corrosion behaviour of G3Si1/G19 9 L Si and 18 L Nb/G19 9 L Si gradient FGMs. Samples were machine from the WAAM wall and submersed in 0.6 M NaCl solution. For the G3Si1/G19 9 L Si material as the material transition occurred the Cr wt% increased and therefore should have had a beneficial increase in corrosion resistance. This did not occur at the expected rates. This was deemed to be from micro-galvanic coupling of

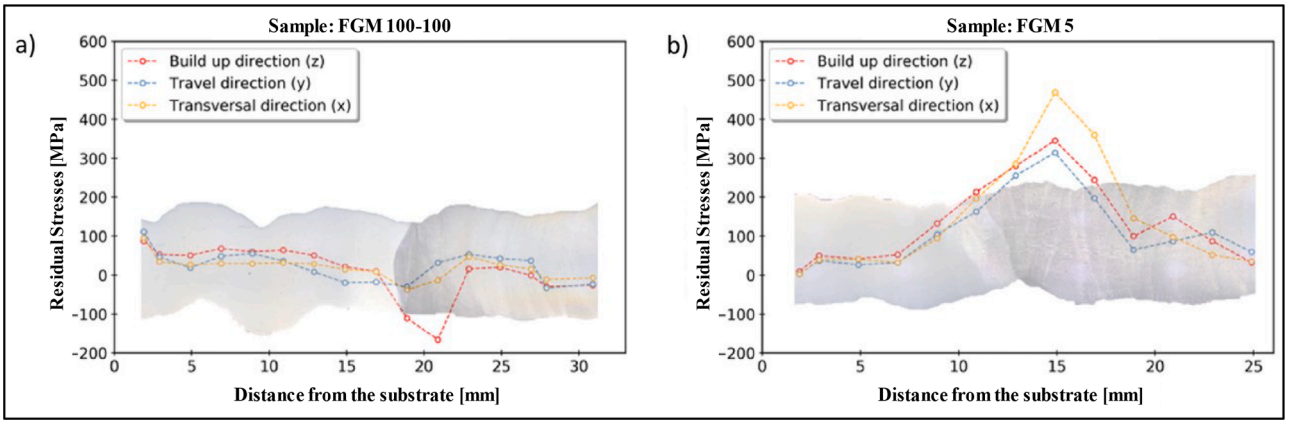

Fig. 34. Residual stresses in the three principal directions: a) FGM 100–100 (Stepped interface); b) FGM 5 (Gradient). [69].

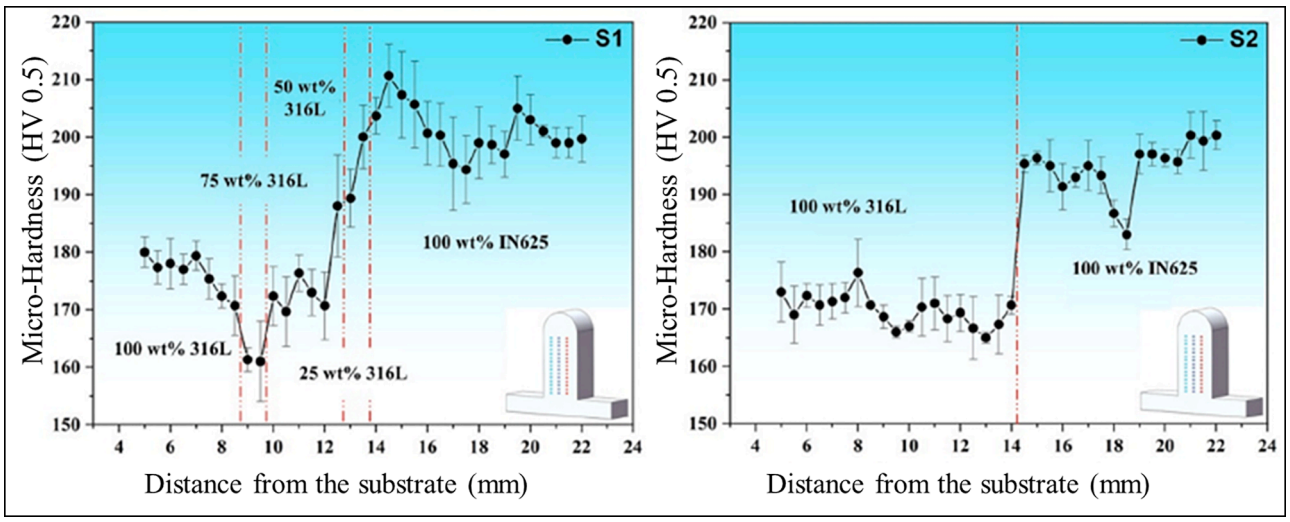

Fig. 35. Micro-Hardness for Gradient (S1) and Stepped (S2) FGMs [70].

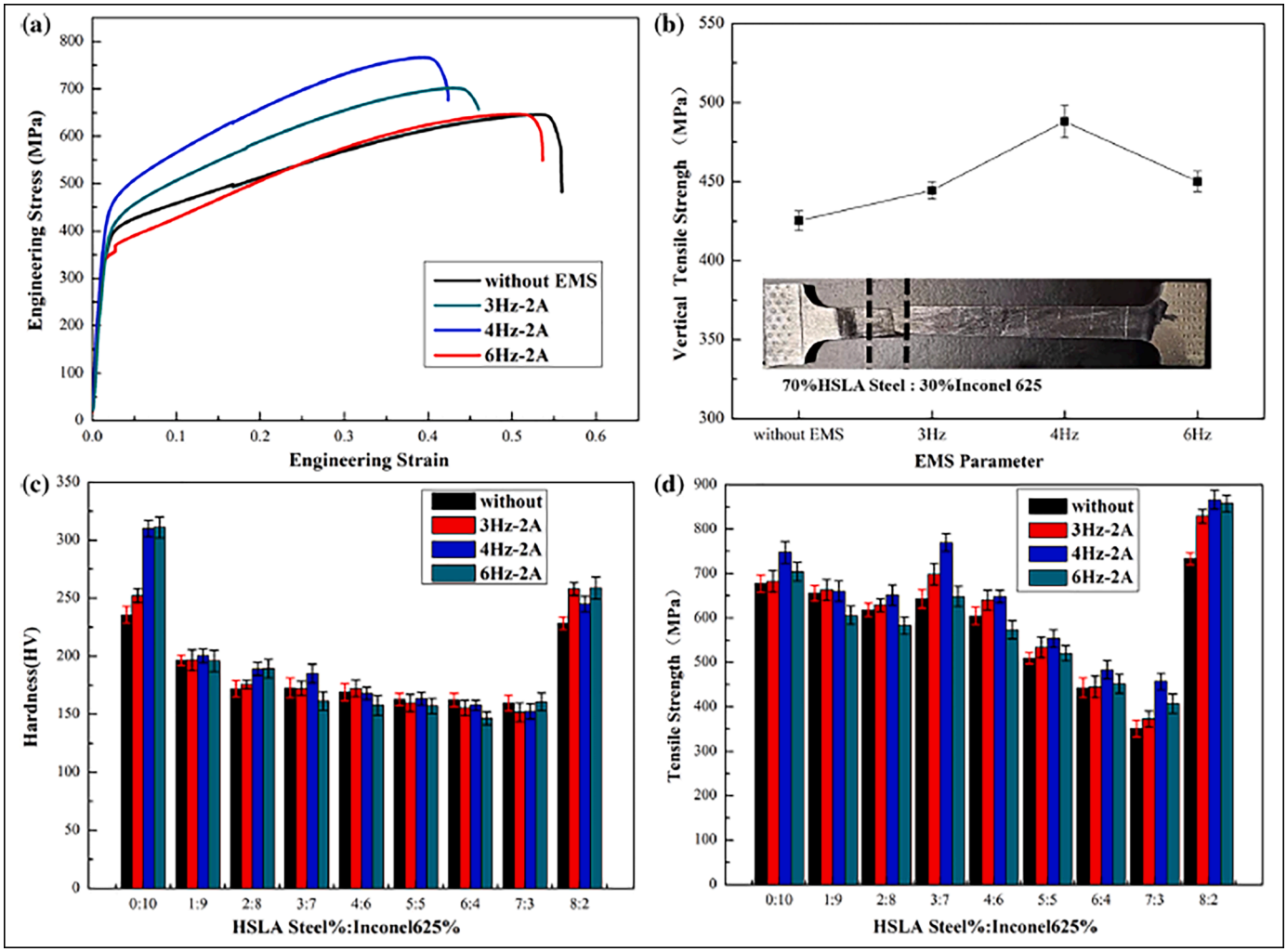

Fig. 36. . Effect of EMS on the mechanical properties of FGMs: (a) engineering stress–strain diagram of FGMs, (b) vertical tensile strength of FGMs fabricated in EMS with different frequencies, (c) microhardness of FGMs fabricated in EMS with different frequencies, (d) tensile strength of FGMs fabricated in EMS with different frequencies. [71].

various phases having a counteract effect on the CR^{3+} ions. For the 18 L Nb/G19 9 L Si material Nickel was increased along the build direction and had a positive effect on the passive oxide layer. The pits morphology was noted to change along the build direction, and this was believed to be due to the interaction of austenitic and δ-ferritic phases causing pit initiation sites at their boundaries. These pits can be seen from OM images in Fig. 37 along with a graph showing pit surface area. All samples were grounded with SiC paper and water, then polished with various diamond pastes. After this samples P1–3 were etched with $CuCl_2$ and P4–5 with KOH before OM could take place [73]. Therefore, it can be said that another gap within literature in the knowledge of the corrosion properties and optimisation WAAM built FGM.

Hybrid AM

A promising area of Additive Manufacturing is hybrid Am that looks to combine different manufacturing processes so that components can be made quicker and more cost effectively. There has been interesting developments with a range of different manufacturing process combinations being investigated. Niu et al. has explored the possibility of combining MIG-WAAM and LDED in one manufacturing process to create components of different properties. From their findings it was proven that the two technologies can be successfully used to manufacture components. The interface between WAAM and LDED regions showed a good metallurgical bond. The LDED produced a finer microstructure and mechanical properties compared to the WAAM with hardness values of 212.88 ± 3.338 $HV_{0.2}$ obtained for the WAAM and 231.88 ± 3.98 $HV_{0.2}$ for the LDED sections. The hybrid material showed better tensile strength than that of the WAAM produced sections with UTS of the different orientations being 648.3 MPa for Scanning Direction (SD), 639.23 MPa for the Transverse Lap Direction (TS) and 623.3 MPa for the Build Direction (BD). The decreasing strength pattern of SD→TD→BD was also noted in the WAAM only region. Fracture always occurred in the WAAM region of the Hybrid specimens showing that the interface has a higher strength than that of the WAAM and all fractures were in the ductile mode. LDED was used in the surface treatment of the WAAM surface to see if the rough surface produced from the WAAM build can be smoothened to reduce the required machining allowance. It was found that a surface defect of 1.5 mm can be reduced to 0.4 mm and therefore reduced the required machining allowance. Fig. 38 provides a schematic of the repair plan along with images comparing with and without the surface repair [74]. This method could prove useful ensuring that less WAAM surface needs to be removed and could improve fatigue resistance due to improve surface quality.

As WAAM does result in a rough surface finish, machining of this is almost always required, therefore combing CNC and WAAM is of great interest. Veiga et al. combined PAW-WAAM with CNC milling in a hybrid manufacturing setup for a Ti6Al4V wall [75]. Up milling and down milling strategies were investigated, and it was found that torque values were similar for both strategies, but up milling provided better surface roughness. Cutting speed affects the torque of the cutting tool. As the depth was increased surface quality was improved. A tool breakage occurred during testing. This is believed to be a result of localised hardening at interface layers and the presence of precipitates in the material [75]. Ghafoori et al. compared WAAM and Hybrid WAAM repair to conventional repair options for structural fatigue cracking maintenance. They found that the fatigue life of the WAAM repair yielded a longer fatigue life lasting to 2.22 million cycles compared to 1.6 million for carbon fibre reinforced polymer (CFRP) and 0.94 million for the sample without repair. However, the fatigue cracking that the WAAM repaired was not the cause of failure. This failed due to a fatigue crack on the WAAM deposited edge as a stress concentration was present. The location of failure along with identified fatigue stages is shown in Fig. 39. After analysis via finite element simulations, the hybrid manufacturing was introduced to machine a pyramid shape after WAAM deposition. This underwent fatigue testing, and no crack initiation was noted after 6 million cycles and an additional 3 million cycles was performed at a higher load and still no cracking was observed. A comparison of these fatigue life results for the reference, CFRP, unmachined WAAM and machined WAAM can be seen in Fig. 40. The success of the WAAM repairs comes from the compressive residual stresses imposed onto the crack tip during cooling as well as the increased surface area providing more stress paths [76].

Forging has been another area investigated but not in as much as CNC-WAAM. Bambach et al. have looked at combining WAAM with forging for Ti-6Al-4 V components for the aerospace industry. Two approaches were adopted, one took a forged component and grew a rib via WAAM creating a FGM. This can be seen in Fig. 41 where SEM images at different locations along the build height are presented. These were

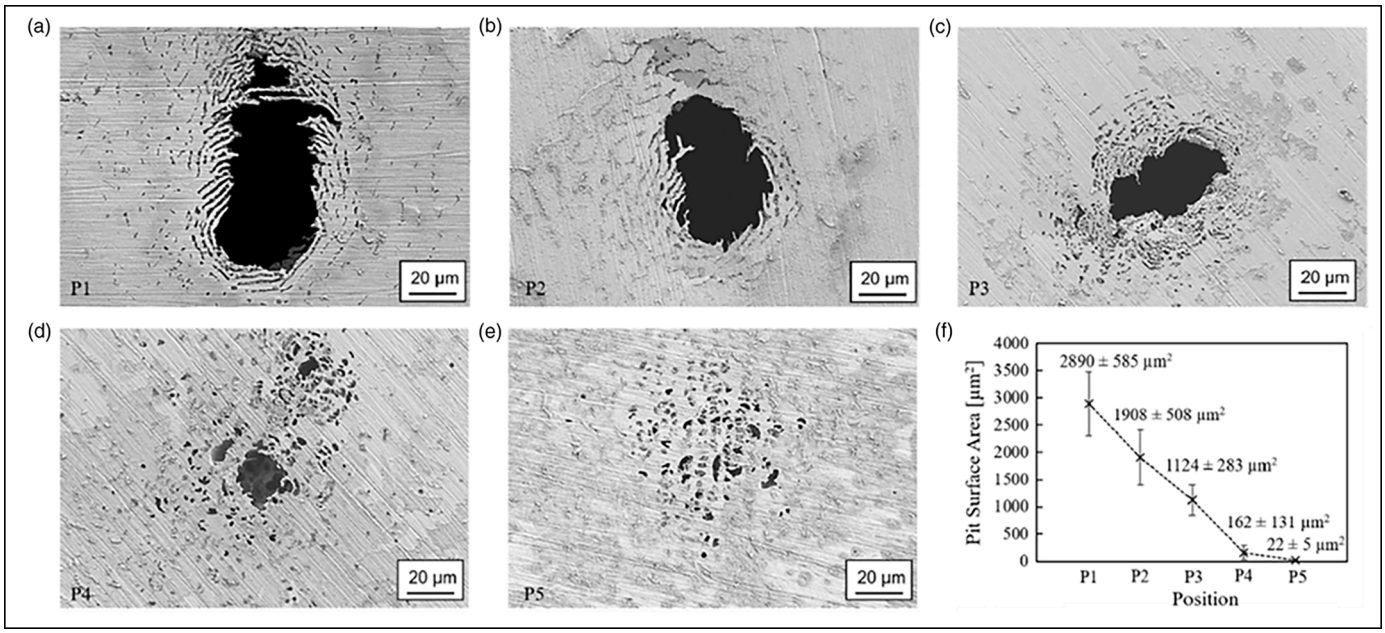

Fig. 37. SEM-SE top view images of C2 P1–P5 a–e) after CPDP and f) the individual pit surface area of P1–P5 determined by quantitative image [73].

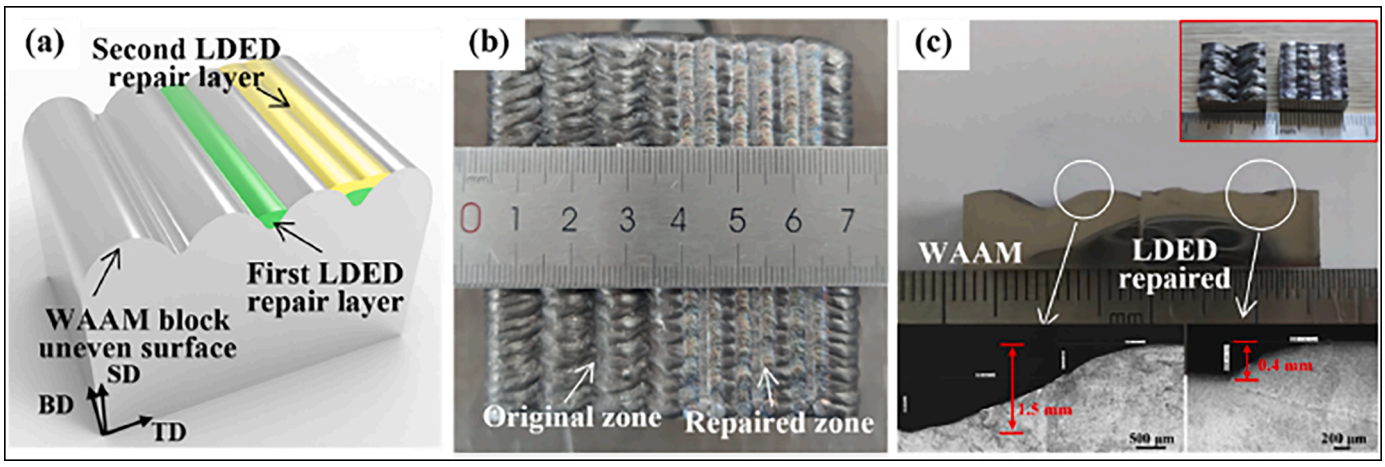

Fig. 38. Repair of uneven side of WAAM block: (a) Repair schematic image, (b) Repair effect, (c) Repair specimen comparison [74].

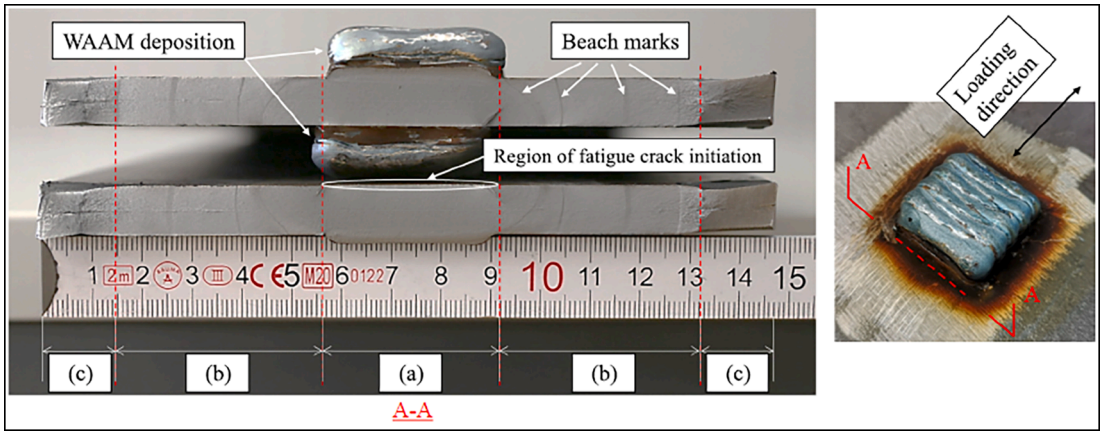

Fig. 39. Fracture surface, i.e., cross-section A-A, of the as-deposited WAAM repair specimen shows three regions: (a) fatigue crack initiation and through thickness propagation, (b) crack propagation through the width direction, and (c) sudden rupture [76].

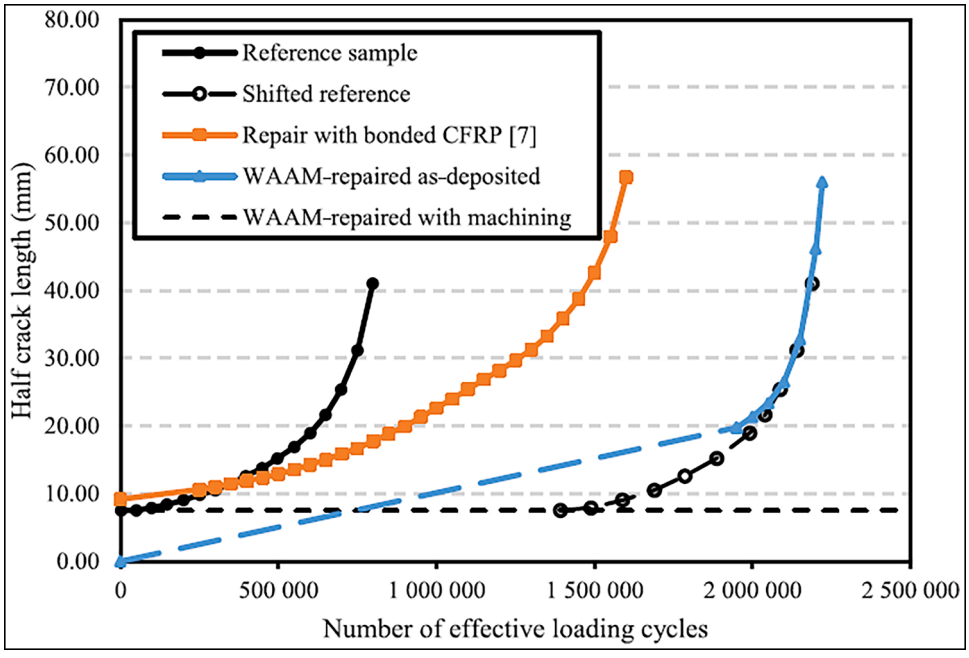

Fig. 40. Fatigue a-N curves of the specimens. The curve with hollow markers is the reference curve shifted by adding 1.39 million cycles [76].

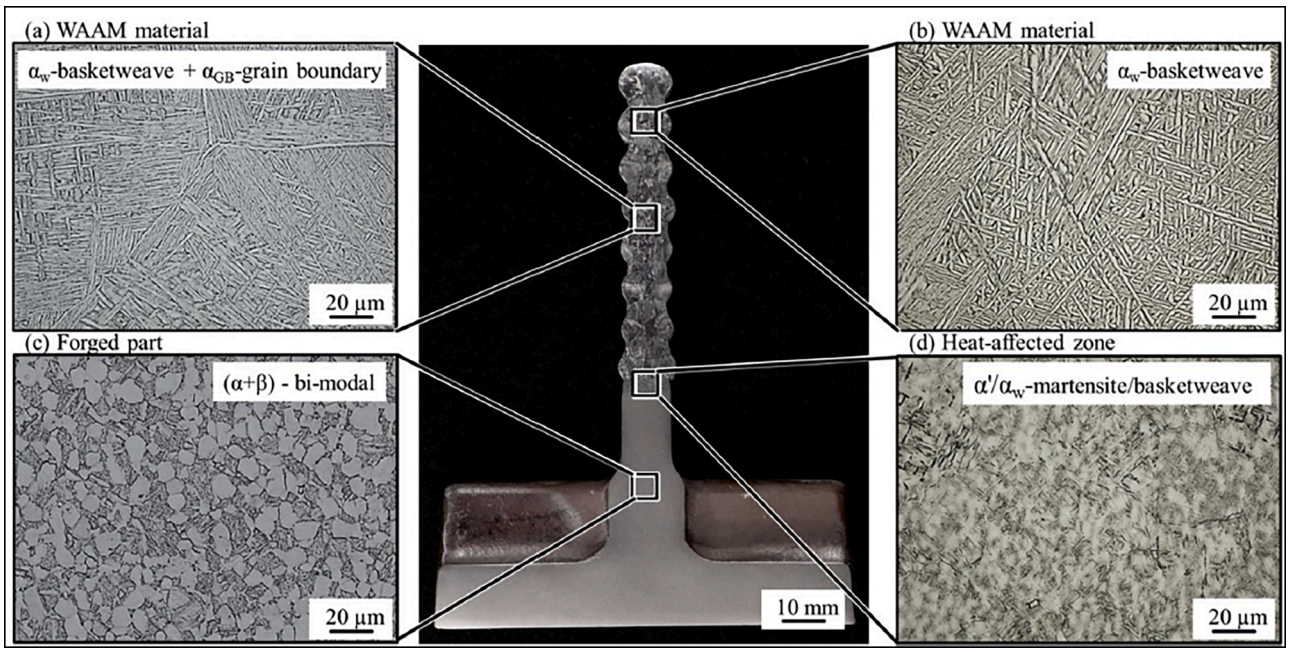

Fig. 41. Microstructure images of WAAM Ti-6Al-4 V material at different positions [77].

prepared via grounding the samples using various grades of silicon carbide paper, then polished with a 0.05 µm silica solution with the additions of H_2O_2, HNO_3, and HF before being etched with Kroll's etching agent. The other approach created an ingot via WAAM, and this used hot forging to create the component. The two components underwent microstructure and mechanical properties investigation. It was found that the FGM had a good interface strength and vertical tensile testing led to failure in the WAAM section. Tensile results showed YS of 842 MPa and UTS of 945 MPa for the WAAM material exceeding the requirements of DIN17864:2023-03 standard for forged components in the aerospace industry of YS: 830 MPA, UTS: 900 MPa. However, the elongation was 7 % and therefore below the 10 % requirement of the standard. The forging of WAAM material yielded even better results with a YS of 922 MPa, UTS 980 MPa and elongation of 14.5 %. This surpasses the standard and shows excellent promise in hybrid manufacturing of forged WAAM, a comparison of both forged variants to DIN17864 can be seen in Fig. 42 [77].

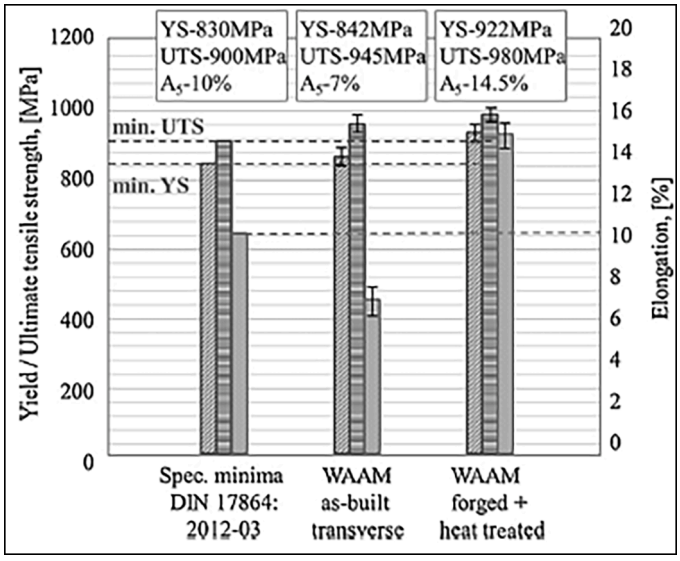

Fig. 42. Average results from tensile testing for different process conditions WAAM transverse to build direction and WAAM forged and heat-treated compared against the specifications minima prescribed for forged Ti-6Al-4 V alloy DIN 17,864:2012–03 [77].

Another aspect of hybrid AM that has been investigated is adding thermal treatments to improve material properties to better combat failure mechanisms and improve manufacturing time. Shen et al. have created a process of in-situ induction heating to affect the residual stress distribution of WAAM build SS308 C beams. A finite element model of the part was created to simulate the thermal cycle of the part from interlayer deposition. From this a stress model was created in ABAQUS to evaluate the stress distribution within the part. Finite element simulation of the induction heating was added to the model to see the change on the stress distribution and find the points in the part with the largest stress change. Two sets of components were made: one in-situ induction heating and one with normal build parameters. The residual stresses were measured via the blind hole method at the identified location from the finite element model. The results showed that the simulation and experiments were closely aligned. It was proven that the in-situ induction heating allows for the targeted change in residual stresses in WAAM built components [78]. This can lead to improved fatigue resistance if carried out correctly.

Heinrich et al. have explored the possibility of decreasing manufacture time for WAAM components via thermal cooling. In hybrid manufacturing the decreased WAAM build time and reduced dwell times between layers can lead to improved manufacturing efficiency and therefore lower cost. The build plate conduction cooling was applied to the manufacture of mild steel rectangular profiles with side cooling at either side of the build and bottom cooling with cooling directly under the build. High deposition rate of 4.5–5 kg/hr was utilised and the build plate was kept at 33 % the temperature of conventional WAAM. From this it was found that side cooling is not effective but bottom cooling can lead to a reduction of 50 % manufacture time. Bottom cooling was applied to build strategies with dwell times of 30, 45 and 60 s and compared them to convention ones. Cross sections are compared in Fig. 43 to highlight the difference in quality. Porosity of the cross sections was evaluated and found that the conventional strategy with a dwell of 30 s resulted in the highest porosity. For the same dwell time in the in-situ cooling had approximately half; this can be seen better detail from Fig. 44 that shows the pore volume and max pore size for each build strategy [79]. However, further study should be conducted to

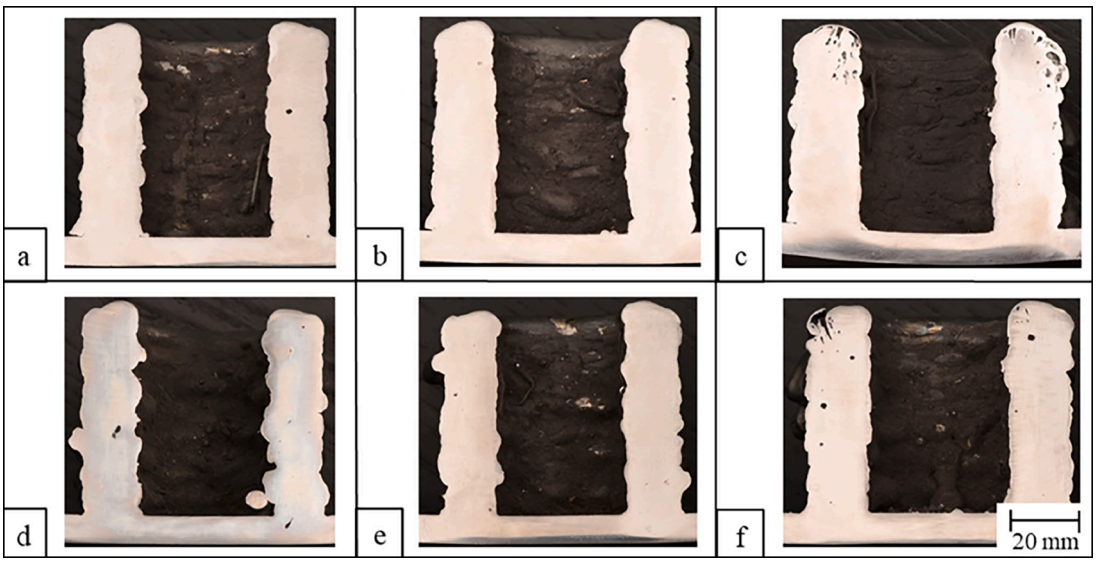

Fig. 43. Cross sections of conventional components at (a) t_C = 60-s, (b) t_C = 45-s, and (c) t_C = 30-s and bottom build plate conduction cooling components with (d) t_B = 60-s, € t_B = 30-s, and (f) t_B = 15-s [79].

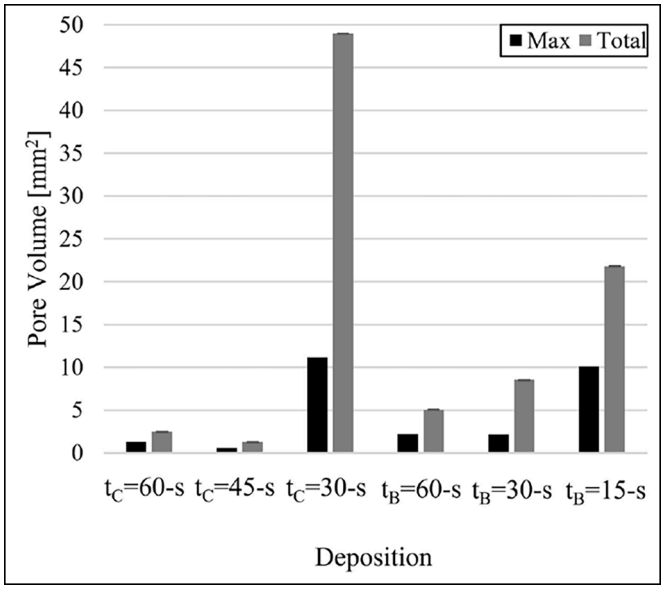

Fig. 44. Porosity total area and maximum pore size generated using [79].

assess the impact on build quality of the materials to see how they are affected.

Multi-material AM build strategies for offshore renewable energy applications

WAAM has shown that it can successfully manufacture materials that have similar mechanical properties to wrought material but depending on manufacturing can show directionality. Similarly, it has been proven that materials can successfully be mixed in order to manufacture FGMs, either stepped or gradient variations. A lot of works focusses on only stepped but gradient methods should be explored in more detail. Initial studies on moving the failure regions to specific locations is very intriguing. In terms of offshore renewable energy structures this method, once finely tuned, could be applied to the design of key components with failure areas that can be inspected rather than whole parts, reducing OPEX.

In terms of combating Fatigue-Corrosion-Erosion FGMs have shown a trend of increased hardness at the interface but this is very much dependent on the material combinations and should be investigated further. However, this could lead to the creation of an erosion resistance surface that is made up from corrosion and fatigue resistant materials that would benefit erosion-corrosion dominate environments. An area that will need to be investigated is the effect of galvanic corrosion on the material due to material mixing. This could lead to detrimental effects therefore should be well understood. Corrosion knowledge is limited for FGMs hence another gap in the knowledge. However, corrosion resistance materials are generally high cost, therefore being able to combine small amounts of corrosion resistant material with a cheaper alloy for the bulk could lead to reductions in material CAPEX.

Using hybrid-AM in the offshore renewable energy sector could prove beneficial to creating components in short lead times, especially if Net Zero targets are to be met. The combination of CNC-WAAM shows great promise to create components with minimal waste and high quality. The process should be examined in more detail for large components as this would be beneficial for ORE structures in terms of both initial components and operational repairs. If components can be made at the port or operation & maintenance base supply chain constraints could be eased. The benefits of in-situ processing such as ultrasonic, heating and cooling could lead to improved manufacturing time and/or microstructures that are more fatigue resistant.

Advantages and disadvantages for the use of WAAM in industry

Within both industry and academia, the question of why WAAM should be used instead of conventional manufacturing techniques for ORE is heavily discussed. One of the major disadvantages is the cost of the process. This, like most technologies, is likely to reduce as expertise and optimisation occurs. However, the advantages of WAAM, detailed in Table 1, outweigh the disadvantages in the eyes of the authors. ORE supply chain often requires long lead times and therefore the ability to manufacture near the site of interest can dramatically reduce these. The performance of the material can also exceed that of the wrought material which can lead to further economic value in terms of extended life and minimal repair. Another area that is of great importance is the reduction in emissions from the manufacturing process when compared to conventional processes [80,81].

Table 1
Advantages and Disadvantages for Wire Arc Additive Manufacturing Process.

Advantages	Disadvantages
Complex parts can be manufactured easily	High cost
Near Net shape can be achieved to reduce wastage	Long manufacturing times compared to some conventional processes
Materials can be mixed to improve properties	High CAPEX required for equipment
FGMs can be produced therefore decreasing material cost	Porosity can be an issue with defects present in components
Manufacturing can be near source reducing supply lead times	Need for post manufacturing machining
Thermal cycles may lead to higher hardness values	Unpredictable residual stress profiles throughout build
Fatigue life can be higher than that of wrought material	Impact on residual stress distribution when separated from base plate
Components can be coated or repaired using WAAM	
Low emissions compared to conventional manufacturing processes	
Higher corrosion resistance is possible through hybrid material creation	
No size constrains on manufacture	
Low energy consumption manufacture	

Conclusion

Within this paper an extensive review of literature has been undertaken and the current and future market trends within the offshore renewable energy and additive manufacturing sectors have been highlighted, showing that the two are in a position to assist the growth of one another. In terms of the knowledge in Additive Manufacturing (AM) for the offshore environment, this has been lacking when compared to other sectors. However, the implementation of research projects and standards for AM in the marine environment showcases the demand from industry. Offshore renewable energy structures are required to last minimum of 20–30 years to achieve low Levelised Cost Of Energy (LCOEs). As such the main degradation methods of the structures has been highlighted to be fatigue, corrosion and erosion. It is therefore important that AM materials properties are investigated in relations to these. Below are the main conclusion points drawn from this study:

- Fatigue-erosion-corrosion interaction is present in the offshore environment. However, this interaction is not looked at in great detail.
- Wire Arc Additive Manufacturing (WAAM) is one of the most promising AM technologies for the offshore renewable energy industry due to fast deposition speeds, ability to create large components and when manufactured correctly, material properties are equal if not greater than that of wrought material.
- A lack of knowledge exists in the corrosion behaviour on WAAM, with current studies focusing on high corrosion resistant materials.
- Erosion knowledge of WAAM is almost non-existent.
- There have been multiple research projects conducted on WAAM in terms of fatigue. However, some studies report fatigue resistance to be better and others report it to be worse than the wrought. This highlights a contradiction that should be investigated further to understand the reasons behind the two trends.
- WAAM can mix materials during manufacture, creating Functionally Graded Materials (FGMs). This allows for tailoring of properties for their application. Stepped FGM have been researched in more detail showing that it possible to mix a variety of materials whilst the gradient strategies have not.
- FGMs via WAAM can create harder material, which would increase the erosion resistance. However, contradictions exist between researchers and should be investigated further.
- Corrosion resistance knowledge of FGMs via WAAM is very limited.
- Hybrid AM has the potential to bring down the cost of WAAM and can make it more appealing to industry. Therefore, it should be investigated further to see how optimisation of materials and processes can be achieved in order to deliver high quality and cost-effective components and structures to the offshore renewable energy sector.

CRediT authorship contribution statement

Fraser O'Neill: Writing – original draft, Validation, Methodology, Investigation, Formal analysis. **Ali Mehmanparast:** Writing – review & editing, Supervision, Funding acquisition, Conceptualization.

Declaration of competing interest

The authors declare that they have no known competing financial interests or personal relationships that could have appeared to influence the work reported in this paper.

Data availability

Data will be made available on request.

Acknowledgements

This work was supported by grant EP/S023801/1 for Strathclyde, Oxford, and Edinburgh Universities Centre for Doctoral Training in Wind and Marine Energy Systems and Structures – WAMSS CDT (https://www.wamss-cdt.co.uk/) from the UK Engineering and Physical Sciences Research Council (EPSRC).

References

[1] "Climate Change (Emissions Reduction Targets) (Scotland) Act 2019," 2040.
[2] Scotland. Scottish Government and APS Group Scotland, Scottish energy strategy : the future of energy in Scotland.
[3] "Offshore wind: sector profile".
[4] D. for Energy Security and N. Zero, "Offshore Wind Net Zero Investment Roadmap".
[5] International Renewable Energy Agency, Offshore renewables : an action agenda for deployment.
[6] R. Biswal, A. Al Mamun, A. Mehmanparast, On the performance of monopile weldments under service loading conditions and fatigue damage prediction, Fatigue Fract. Eng. Mater. Struct. 44 (6) (Jun. 2021) 1469–1483, https://doi.org/10.1111/ffe.13442.
[7] O. Gaidai, V. Yakimov, F. Wang, F. Zhang, R. Balakrishna, Floating wind turbines structural details fatigue life assessment, Sci. Rep. 13 (1) (Dec. 2023), https://doi.org/10.1038/s41598-023-43554-4.
[8] S. Ambühl, "Reliability of Wave Energy Converters Revised Version of Civil Engineering".
[9] L. Chen, W.H. Lam, A review of survivability and remedial actions of tidal current turbines, in: Renewable and Sustainable Energy Reviews, 43, Elsevier Ltd, 2015, pp. 891–900, https://doi.org/10.1016/j.rser.2014.11.071.
[10] C.A. Douglas, G.P. Harrison, J.P. Chick, Life cycle assessment of the Seagen marine current turbine, Proc. Inst. Mech. Eng. Part M J. Eng. Maritime Environ. 222 (1) (2008) 1–12, https://doi.org/10.1243/14750902JEME94.
[11] D. Dunnett, J.S. Wallace, Electricity generation from wave power in Canada, Renew. Energy 34 (1) (Jan. 2009) 179–195, https://doi.org/10.1016/j.renene.2008.04.034.
[12] "Guide to an offshore wind farm Updated and extended Published on behalf of The Crown Estate and the Offshore Renewable Energy Catapult The Crown Estate Offshore Renewable Energy Catapult," 2019. [Online]. Available: www.thecrownestate.co.uk.
[13] T. T. Wohlers, Wohlers report 2023 : 3D printing and additive manufacturing global state of the industry. 2023.
[14] "Aerospace AM Insights From the stratosphere to space," 2022. [Online]. Available: www.3dpbm.com.
[15] "AM Sustainability Insights The time for ecological solutions is now," 2021. [Online]. Available: www.3dpbm.com.
[16] B.K. Post et al., "A Comparative Study of Direct and Indirect Additive Manufacturing Approaches for the Production of a Wind Energy Component." [Online]. Available: www.osti.gov.
[17] O.B.E. Moe, D. . Bertrand, and H.B. Maillon, "OTC-30971-MS Qualification of AM-Parts for The Offshore Industry," 2021. [Online]. Available: http://onepetro.org/

OTCONF/proceedings-pdf/21OTC/1-21OTC/D011S013R007/2523357/otc-30971-ms.pdf/1.
[18] R. Baker, "Method of making decorative articles," 1925.
[19] T. Wohlers and T. Gornet, "History of Additive Manufacturing," 2015.
[20] Handbook of Post-Processing in Additive Manufacturing.
[21] "Additive manufacturing-General principles-Fundamentals and vocabulary 1,2." [Online]. Available: https://www.iso.org/obp.
[22] S. Chaudhary, S.K. Avinashi, J. Rao, C. Gautam, Recent Advances in Additive Manufacturing, Applications and Challenges for Dentistry: A Review, ACS Biomater. Sci. Eng. 9 (7) (Jul. 2023) 3987–4019, https://doi.org/10.1021/acsbiomaterials.2c01561.
[23] by Siemens, "Press Joint Press Release," 2017. [Online]. Available: www.siemens.com/press/PR2017120112PGEN.
[24] C. Nota, G. Rückert, J.L. Heuzé, L. Carlino, J.M. Quenez, L. Courregelongue, A first feedback on manufacturing and in-service behaviour of a WAAM-made propeller for naval application, Welding in the World 67 (4) (Apr. 2023) 1113–1121, https://doi.org/10.1007/s40194-023-01475-w.
[25] Supergen ORE Hub Flex Fund Project Corrosion and fatigue protection of offshore wind Turbine structures using additive manufacturing technology (COATing).
[26] J. Schijve, "Fatigue of Structures and Materials," 2009.
[27] G.W. Stachowiak and A.W. Batchelor, "Engineering Tribology," 2014. Accessed: Jan. 08, 2024. [Online]. Available: https://www.sciencedirect.com/book/9780123970473/engineering-tribology.
[28] J.B. Singh, "Materials Horizons: From Nature to Nanomaterials Alloy 625 Microstructure, Properties and Performance." [Online]. Available: https://link.springer.com/bookseries/16122.
[29] G. Grasu, P. Liu, Risk assessment of Floating Offshore Wind Turbine, Energy Reports 9 (Dec. 2023) 1–18, https://doi.org/10.1016/j.egyr.2022.11.147.
[30] J. Orlikowski, M. Szociński, K. Żakowski, P. Igliński, K. Domańska, K. Darowicki, Actual field corrosion rate of offshore structures in the Baltic Sea along depth profile from water surface to sea bed, Ocean Engineering 265 (Dec. 2022), https://doi.org/10.1016/j.oceaneng.2022.112545.
[31] W. Khodabux, P. Causon, F. Brennan, Profiling corrosion rates for offshorewind turbines with depth in the North Sea, Energies (Basel) 13 (10) (May 2020), https://doi.org/10.3390/en13102518.
[32] Z.H. Tian, Y.T. Zhao, Y.J. Jiang, H.P. Ren, Microstructure and properties of Inconel 625 + WC composite coatings prepared by laser cladding, Rare Metals 40 (8) (Aug. 2021) 2281–2291, https://doi.org/10.1007/s12598-020-01507-0.
[33] V. Rajkumar, M. Vishnukumar, M. Sowrirajan, A. Rajesh Kannan, Microstructure, mechanical properties and corrosion behaviour of Incoloy 825 manufactured using wire arc additive manufacturing, Vacuum. 203 (Sep. 2022), https://doi.org/10.1016/j.vacuum.2022.111324.
[34] M. Vishnukumar, R. Pramod, A. Rajesh Kannan, Wire arc additive manufacturing for repairing aluminium structures in marine applications, Mater. Lett. 299 (Sep. 2021), https://doi.org/10.1016/j.matlet.2021.130112.
[35] A.R. Kannan, S.M. Kumar, R. Pramod, N.S. Shanmugam, M. Vishnukumar, S. G. Channabasavanna, Microstructure and corrosion resistance of Ni-Cu alloy fabricated through wire arc additive manufacturing, Mater. Lett. 308 (Feb. 2022), https://doi.org/10.1016/j.matlet.2021.131262.
[36] A. Rajesh Kannan, N. Siva Shanmugam, V. Rajkumar, M. Vishnukumar, Insight into the microstructural features and corrosion properties of wire arc additive manufactured super duplex stainless steel (ER2594), Mater. Lett. 270 (Jul. 2020), https://doi.org/10.1016/j.matlet.2020.127680.
[37] A. Queguineur, G. Rückert, F. Cortial, J.Y. Hascoët, Evaluation of wire arc additive manufacturing for large-sized components in naval applications, Welding in the World 62 (2) (Mar. 2018) 259–266, https://doi.org/10.1007/s40194-017-0536-8.
[38] A. Ermakova, A. Mehmanparast, Corrosion Effects on Fracture Toughness Properties of Wire Arc Additively Manufactured Low Carbon Steel Specimens, Metals (Basel) 12 (2) (Feb. 2022), https://doi.org/10.3390/met12020238.
[39] E. Hassan, et al., Erosion mapping of through-thickness toughened powder epoxy gradient glass-fiber-reinforced polymer (GFRP) plates for tidal turbine blades, Lubricants 9 (3) (Mar. 2021) 1–22, https://doi.org/10.3390/lubricants9030022.
[40] Y. Xu, et al., Flow accelerated corrosion and erosion−corrosion behavior of marine carbon steel in natural seawater, NPJ Mater. Degrad. 5 (1) (Dec. 2021), https://doi.org/10.1038/s41529-021-00205-1.
[41] W. Wang, et al., Understanding the effect of tensile stress on erosion-corrosion of X70 pipeline steel, Constr. Build. Mater. 342 (Aug. 2022), https://doi.org/10.1016/j.conbuildmat.2022.127972.
[42] H. Shahali, H.M. Ghasemi, M. Abedini, Contributions of corrosion and erosion in the erosion-corrosion of Sanicro28, Mater. Chem. Phys. 233 (May 2019) 366–377, https://doi.org/10.1016/j.matchemphys.2019.05.051.
[43] M. Shamir, J. Braithwaite, A. Mehmanparast, Fatigue life assessment of offshore wind support structures in the presence of corrosion pits, Marine Structures 92 (Nov. 2023), https://doi.org/10.1016/j.marstruc.2023.103505.
[44] T. Papatheocharis, G.C. Sarvanis, P.C. Perdikaris, S.A. Karamanos, A.D. Zervaki, Fatigue resistance of welded steel tubular X-joints, Marine Structures 74 (Nov. 2020), https://doi.org/10.1016/j.marstruc.2020.102809.
[45] K. Chatziioannou, S.A. Karamanos, Y. Huang, Ultra low-cycle fatigue performance of S420 and S700 steel welded tubular X-joints, Int. J. Fatigue 129 (Dec. 2019), https://doi.org/10.1016/j.ijfatigue.2019.105221.
[46] J. López-Queija, E. Robles, J. Jugo, S. Alonso-Quesada, Review of control technologies for floating offshore wind turbines, Renewable and Sustainable Energy Reviews 167 (Oct. 01, 2022), https://doi.org/10.1016/j.rser.2022.112787.
[47] M. Ramezani, D.E. Choe, K. Heydarpour, B. Koo, Uncertainty models for the structural design of floating offshore wind turbines: A review, in: Renewable and Sustainable Energy Reviews, 185, Elsevier Ltd, 2023, https://doi.org/10.1016/j.rser.2023.113610. Oct. 01.
[48] T. Zou, X. Niu, X. Ji, M. Li, L. Tao, The impact of initial imperfections on the fatigue assessment of tower flange connections in floating wind turbines: A review, Front. Mar. Sci. 9 (Nov. 14, 2022), https://doi.org/10.3389/fmars.2022.1063120. Frontiers Media S.A.
[49] H. Mullings, T. Stallard, Assessment of dependency of unsteady onset flow and resultant tidal turbine fatigue loads on measurement position at a tidal site, Energies (Basel) 14 (17) (Sep. 2021), https://doi.org/10.3390/en14175470.
[50] T. Papatheocharis, G.T. Plakias, A.D. Zervaki, P.C. Perdikaris, S.A. Karamanos, Ultimate strength and fatigue of stiffened welded tubular joints in floating energy production structures, Eng. Struct. 297 (Dec. 2023), https://doi.org/10.1016/j.engstruct.2023.116985.
[51] Z. Shahroozi, M. Göteman, J. Engström, Fatigue analysis of a point-absorber wave energy converter based on augmented data from a WEC-Sim model calibrated with experimental data. Trends in Renewable Energies Offshore - Proceedings of the 5th International Conference On Renewable Energies Offshore, RENEW 2022, CRC Press/Balkema, 2023, pp. 925–933, https://doi.org/10.1201/9781003360773-102.
[52] A. Ermakova, J. Razavi, R. Crescenzo, F. Berto, A. Mehmanparast, Fatigue life assessment of wire arc additively manufactured ER100S-1 steel parts, Progress in Additive Manufacturing (2023), https://doi.org/10.1007/s40964-023-00400-3.
[53] A. Ermakova, A. Mehmanparast, S. Ganguly, J. Razavi, F. Berto, Fatigue crack growth behaviour of wire and arc additively manufactured ER70S-6 low carbon steel components, Int. J. Fract. 235 (1) (May 2022) 47–59, https://doi.org/10.1007/s10704-021-00545-8.
[54] G.A. Webster, et al., Fatigue characterization of wire arc additive manufactured AWS ER100S-G steel: fully reversed condition, Eng. Fail. Anal. 153 (Nov. 2023), https://doi.org/10.1016/j.engfailanal.2023.107562.
[55] Y. Ayan, N. Kahraman, Bending fatigue properties of structural steel fabricated through wire arc additive manufacturing (WAAM, Eng. Sci. Tech. Int. J. 35 (Nov. 2022), https://doi.org/10.1016/j.jestch.2022.101247.
[56] C. Huang, L. Li, N. Pichler, E. Ghafoori, L. Susmel, L. Gardner, Fatigue testing and analysis of steel plates manufactured by wire-arc directed energy deposition, Addit. Manuf. 73 (Jul. 2023), https://doi.org/10.1016/j.addma.2023.103696.
[57] J. He, X. Feng, X. Wang, X. Guan, Fatigue performance and acoustic emission behavior of remanufactured low-carbon steel made by wire and arc additive manufacturing, Int. J. Fatigue 165 (Dec. 2022), https://doi.org/10.1016/j.ijfatigue.2022.107190.
[58] T. Ron, G.K. Levy, O. Dolev, A. Leon, A. Shirizly, E. Aghion, The effect of microstructural imperfections on corrosion fatigue of additively manufactured ER70S-6 alloy produced by wire arc deposition, Metals (Basel) 10 (1) (Jan. 2020), https://doi.org/10.3390/met10010098.
[59] F. Ji, Z. Hu, X. Qin, F. Yin, M. Ni, X. Xiong, Grain refinement and mechanism of steel in ultrasound assisted wire and arc additive manufacturing, Int. Commun. Heat Mass Transf. 143 (Apr. 2023), https://doi.org/10.1016/j.icheatmasstransfer.2023.106724.
[60] C.B. von der Ohe, R. Johnsen, N. Espallargas, Modeling the multi-degradation mechanisms of combined tribocorrosion interacting with static and cyclic loaded surfaces of passive metals exposed to seawater, Wear 269 (7–8) (Aug. 2010) 607–616, https://doi.org/10.1016/j.wear.2010.06.010.
[61] J. Zhang, C. Li, L. Ba, X. Di, Transition Strategy Optimization of Inconel625-HSLA Steel Functionally Graded Material Fabricated by Wire Arc Additive Manufacturing, Met. Mater. Int. 29 (3) (Mar. 2023) 767–776, https://doi.org/10.1007/s12540-022-01247-z.
[62] Y. Ayan, N. Kahraman, Fabrication and characterization of functionally graded material (FGM) structure containing two dissimilar steels (ER70S-6 and 308LSi) by wire arc additive manufacturing (WAAM), Mater. Today Commun. 33 (Dec. 2022), https://doi.org/10.1016/j.mtcomm.2022.104457.
[63] Y. Ayan, N. Kahraman, Fabrication and Fatigue Properties of Dissimilar Steel Functionally Graded Material Structure Through Wire Arc Additive Manufacturing, J. Mater. Eng. Perform. (2023), https://doi.org/10.1007/s11665-023-07914-5.
[64] S. Chandrasekaran, S. Hari, M. Amirthalingam, Wire arc additive manufacturing of functionally graded material for marine risers, Materials Science and Engineering: A 792 (Aug. 2020), https://doi.org/10.1016/j.msea.2020.139530.
[65] S. Mohan Kumar, et al., Microstructural Features and Mechanical Integrity of Wire Arc Additive Manufactured SS321/Inconel 625 Functionally Gradient Material, J. Mater. Eng. Perform. 30 (8) (Aug. 2021) 5692–5703, https://doi.org/10.1007/s11665-021-05617-3.
[66] R. Sasikumar, et al., Wire arc additive manufacturing of functionally graded material with SS 316 L and IN625: Microstructural and mechanical perspectives, CIRP J. Manuf. Sci. Technol. 38 (Aug. 2022) 230–242, https://doi.org/10.1016/J.CIRPJ.2022.05.005.
[67] A. Rajesh Kannan, S. Mohan Kumar, N. Pravin Kumar, N. Siva Shanmugam, A. S. Vishnu, Y. Palguna, Process-microstructural features for tailoring fatigue strength of wire arc additive manufactured functionally graded material of SS904L and Hastelloy C-276, Mater. Lett. 274 (Sep. 2020), https://doi.org/10.1016/j.matlet.2020.127968.
[68] T.A. Rodrigues, et al., Steel-copper functionally graded material produced by twin-wire and arc additive manufacturing (T-WAAM, Mater. Des. 213 (Jan. 2022), https://doi.org/10.1016/j.matdes.2021.110270.
[69] T.A. Rodrigues, et al., Wire and arc additive manufacturing of 316 L stainless steel/Inconel 625 functionally graded material: Development and characterization, J. Mater. Res. Technol. 21 (Nov. 2022) 237–251, https://doi.org/10.1016/j.jmrt.2022.08.169.

[70] X. Yu, et al., Effect of composition gradient design on microstructure and mechanical properties of dual-wire plasma arc additively manufactured 316 L/IN625 functionally graded materials, Mater. Chem. Phys. 307 (Oct. 2023), https://doi.org/10.1016/j.matchemphys.2023.128121.
[71] J. Zhang, X. Di, C. Li, L. Ba, X. Jiang, Effect of Electromagnetic Stirring Frequency on Inconel625-High Strength Low Alloy Steel Functionally Graded Material Fabricated by Wire Arc Additive Manufacturing, J. Mater. Eng. Perform. 31 (12) (Dec. 2022) 9703–9713, https://doi.org/10.1007/s11665-022-07008-8.
[72] J. Zhang, et al., In-situ heat treatment (IHT) wire arc additive manufacturing of Inconel625-HSLA steel functionally graded material, Mater. Lett. 330 (Jan. 2023), https://doi.org/10.1016/j.matlet.2022.133326.
[73] R.D. Pütz, Y. Pratesa, L. Oster, R. Sharma, U. Reisgen, D. Zander, Microstructure and Corrosion Behavior of Functionally Graded Wire Arc Additive Manufactured Steel Combinations, Steel. Res. Int. 92 (12) (Dec. 2021), https://doi.org/10.1002/srin.202100387.
[74] F. Niu, W. Bi, K. Zhang, X. Sun, G. Ma, D. Wu, Additive manufacturing of 304 stainless steel integrated component by hybrid WAAM and LDED, Mater. Today Commun. 35 (Jun. 2023), https://doi.org/10.1016/j.mtcomm.2023.106227.
[75] F. Veiga, A.G. Del Val, A. Suárez, U. Alonso, Analysis of the machining process of titanium Ti6Al-4 V parts manufactured by wire arc additive manufacturing (WAAM), Materials 13 (3) (Feb. 2020), https://doi.org/10.3390/ma13030766.
[76] E. Ghafoori, et al., Fatigue strengthening of damaged steel members using wire arc additive manufacturing, Eng. Struct. 284 (Jun. 2023), https://doi.org/10.1016/j.engstruct.2023.115911.
[77] M. Bambach, I. Sizova, B. Sydow, S. Hemes, F. Meiners, Hybrid manufacturing of components from Ti-6Al-4 V by metal forming and wire-arc additive manufacturing, J. Mater. Process. Technol. 282 (Aug. 2020), https://doi.org/10.1016/j.jmatprotec.2020.116689.
[78] H. Shen, J. Lin, Z. Zhou, B. Liu, Effect of induction heat treatment on residual stress distribution of components fabricated by wire arc additive manufacturing, J. Manuf. Process. 75 (Mar. 2022) 331–345, https://doi.org/10.1016/j.jmapro.2022.01.018.
[79] L. Heinrich, T. Feldhausen, K. Saleeby, T. Kurfess, C. Saldaña, Build plate conduction cooling for thermal management of wire arc additive manufactured components, Int. J. Adv. Manuf. Tech. 124 (5–6) (Jan. 2023) 1557–1567, https://doi.org/10.1007/s00170-022-10558-9.
[80] S. Kokare, J.P. Oliveira, R. Godina, A LCA and LCC analysis of pure subtractive manufacturing, wire arc additive manufacturing, and selective laser melting approaches, J. Manuf. Process. 101 (Sep. 08, 2023) 67–85, https://doi.org/10.1016/j.jmapro.2023.05.102. Elsevier Ltd.
[81] R.C. Reis, S. Kokare, J.P. Oliveira, J.C.O. Matias, R. Godina, Life cycle assessment of metal products: A comparison between wire arc additive manufacturing and CNC milling, Adv. Indust. Manuf. Eng. 6 (May 2023), https://doi.org/10.1016/j.aime.2023.100117.
[82] T.S. Senthil, M. Puviyarasan, S Ramesh Babu, T. Ram Prabhu, Pitting corrosion studies on functionally graded Inconel 825-SS316L wall manufactured by wire arc additive manufacturing, Eng. Res. Express 4 (3) (Sep. 2022), https://doi.org/10.1088/2631-8695/ac8148.